JGR Atmospheres

RESEARCH ARTICLE
10.1029/2023JD039492

Key Points:

- Thirteen of eighteen flash rate parameterization schemes overestimated the observed number of flashes by more than 100%
- Upward cloud ice flux and updraft volume schemes well represent lightning activity in the early and later stages of the storm, respectively
- Flash rate prediction is highly dependent on how schemes are applied in cloud-resolved models and on accurate simulation of storm variables

Correspondence to:

K. A. Cummings,
kristin.a.smith@nasa.gov

Citation:

Cummings, K. A., Pickering, K. E., Barth, M. C., Bela, M. M., Li, Y., Allen, D., et al. (2024). Evaluation of lightning flash rate parameterizations in a cloud-resolved WRF-Chem simulation of the 29–30 May 2012 Oklahoma severe supercell system observed during DC3. *Journal of Geophysical Research: Atmospheres*, *129*, e2023JD039492. https://doi.org/10.1029/2023JD039492

Received 19 JUN 2023
Accepted 22 FEB 2024

Evaluation of Lightning Flash Rate Parameterizations in a Cloud-Resolved WRF-Chem Simulation of the 29–30 May 2012 Oklahoma Severe Supercell System Observed During DC3

K. A. Cummings[1,2], K. E. Pickering[1], M. C. Barth[3], M. M. Bela[4,5,6,7], Y. Li[1,8], D. Allen[1], E. Bruning[9], D. R. MacGorman[10,11,12], C. L. Ziegler[10,11], M. I. Biggerstaff[11], B. Fuchs[13,14], T. Davis[13,15], L. Carey[16], R. M. Mecikalski[16], and D. L. Finney[17,18]

[1]Department of Atmospheric and Oceanic Science, University of Maryland, College Park, MD, USA, [2]Now at NASA Kennedy Space Center, FL, USA, [3]National Center for Atmospheric Research, Boulder, CO, USA, [4]Department of Atmospheric and Oceanic Sciences and Laboratory for Atmospheric and Space Physics, University of Colorado Boulder, Boulder, CO, USA, [5]Cooperative Institute for Research in Environmental Sciences, University of Colorado Boulder, Boulder, CO, USA, [6]NOAA Chemical Sciences Laboratory (CSL), Boulder, CO, USA, [7]Now at Geo Sustainability, Google, Boulder, CO, USA, [8]Now at Department of Atmospheric, Oceanic, and Earth Sciences, George Mason University, Fairfax, VA, USA, [9]Department of Geosciences, Texas Tech University, Lubbock, TX, USA, [10]NOAA National Severe Storms Laboratory, Norman, OK, USA, [11]School of Meteorology, University of Oklahoma, Norman, OK, USA, [12]Now at Cooperative Institute for Severe and High-Impact Weather Research and Operations, Norman, OK, USA, [13]Department of Atmospheric Science, Colorado State University, Fort Collins, CO, USA, [14]Now at WeatherFlow Inc., Scotts Valley, CA, USA, [15]Now at National Weather Service, Mt. Holly, NJ, USA, [16]Department of Atmospheric and Earth Science, The University of Alabama in Huntsville, Huntsville, AL, USA, [17]School of Earth and Environment, University of Leeds, Leeds, UK, [18]Ronin Institute for Independent Scholarship, Montclair, NJ, USA

Abstract Eighteen lightning flash rate parameterization schemes (FRPSs) were investigated in a Weather Research and Forecasting model coupled with chemistry cloud-resolved simulation of the 29–30 May 2012 supercell storm system observed during the Deep Convective Clouds and Chemistry (DC3) field campaign. Most of the observed storm's meteorological conditions were well represented when the model simulation included both convective damping and lightning data assimilation techniques. Newly-developed FRPSs based on DC3 radar observations and Lightning Mapping Array data are implemented in the model, along with previously developed schemes from the literature. The schemes are based on relationships between lightning and various kinematic, structural, and microphysical thunderstorm characteristics (e.g., cloud top height, hydrometeors, reflectivity, and vertical velocity) available in the model. The results suggest the model-simulated graupel and snow/ice hydrometeors require scaling factors to more closely represent proxy observations. The model-simulated lightning flash trends and total flashes generated by each scheme over the simulation period are compared with observations from the central Oklahoma Lightning Mapping Array. For this supercell system, 13 of the 18 schemes overpredicted flashes by >100% with the group of FRPSs based on storm kinematics and structure (particularly updraft volume) performing slightly better than the hydrometeor-based schemes. During the storm's first 4 hr, the upward cloud ice flux FRPS, which is based on the combination of vertical velocity and hydrometeors, well represents the observed total flashes and flash rate trend; while, the updraft volume scheme well represents the observed flash rate peak and subsequent sharp decline in flash rate.

Plain Language Summary Accurate lightning forecasts are important for daily activities. They are also important because lightning produces nitrogen oxide, which affects the distribution of atmospheric trace gases that have significant roles in influencing our climate (e.g., ozone). Lightning is recreated in weather models using already determined relationships between observed lightning and thunderstorm characteristics (e.g., hydrometeors and vertical velocity). Lightning prediction is also highly dependent on how well the model represents current conditions, like thunderstorm location and strength. Eighteen lightning-thunderstorm relationships, or schemes, were investigated in a cloud-resolved Weather Research and Forecasting model coupled with chemistry to simulate the 29–30 May 2012 supercell storm system observed during the Deep Convective Clouds and Chemistry (DC3) field campaign and to identify the best scheme associated with the event. Modifications to the model-simulation were first required to better represent the observed convection

before comparing the observed and model-simulated lightning. Generally, the schemes based on storm kinematics and structure perform slightly better for this case study than the microphysical schemes. Two schemes (i.e., upward cloud ice flux and updraft volume) well represent the supercell system's lightning activity. The upward cloud ice flux scheme was used in follow-on lightning chemistry and trace gas analyses.

1. Introduction

Lightning prediction is desirable in weather forecasting models and is necessary in chemistry and climate models for estimating lightning-generated nitrogen oxides (LNO_x). Prior to the 1970s the lack of adequate detection techniques made it difficult to analyze global lightning activity or determine relationships between lightning and storm parameters that could be employed in prediction schemes; however, lightning detection instrumentation has evolved over time. The first optical sensor that orbited Earth could only observe lightning at night (Orville & Henderson, 1986; Turman, 1978). Over the next 40 years advancements in lightning detection technology (e.g., optical, magnetic direction finding, and time-of-arrival sensors) allowed for improvements in detection efficiency, spatial accuracy, the ability to distinguish between cloud-to-ground (CG) and intracloud (IC) lightning, and 3-dimensional (3-D) mapping of total lightning activity (Christian et al., 2003; Cummins & Murphy, 2009; Heckman & Liu, 2010; Krehbiel et al., 2000; Liu & Heckman, 2011; Rison et al., 1999; Thomas et al., 2004).

The availability of high-detection-efficiency flash data, together with radar observations or model data, has allowed the development of lightning flash rate parameterization schemes (FRPSs; relationships between thunderstorm characteristics and lightning activity) to estimate lightning flash rates and location. Currently lightning threat forecasts (McCaul et al., 2009, 2020) are being run in operational models to predict lightning flash rate densities in short-range weather forecasts (i.e., 12–72 hr). These models include the Weather Research and Forecasting (WRF) model as implemented by the National Severe Storms Laboratory (NSSL) (McCaul et al., 2020), the National Oceanic and Atmospheric Administration (NOAA)/National Centers for Environmental Prediction (NCEP) High-Resolution Rapid Refresh (HRRR) model (Benjamin et al., 2016), the National Center for Atmospheric Research (NCAR) ensemble forecast (Schwartz et al., 2015), and the United Kingdom (UK) Met Office UK-variable resolution (UKV) model (Wilkinson & Bornemann, 2014). Lopez (2016) developed a lightning parameterization based on hydrometeors, convective available potential energy (CAPE), and cloud-base height that is used in the European Centre for Medium-Range Weather Forecasting (ECMWF) Integrated Forecasting System. Giannaros et al. (2017) evaluated operational lightning forecasts in Central-South Europe using the WRF model with a convective parameterization and FRPS based on cloud top height (Price & Rind, 1992). Such forecasts are beneficial from an operations and public safety perspective for those individuals who are required or plan to spend an extended amount of time outdoors (e.g., construction, lawn care, airports, rocket launch preparations, and recreational activities). In addition to forecasting future lightning activity, FRPSs may be used to reproduce flash rates from past convective events to verify their performance against lightning observations (Barthe et al., 2010), generate model-simulated flash counts in areas where observed lightning data are unavailable, or use observed total lightning activity to estimate storm parameters that are not routinely measured or observed in real-time (e.g., cloud top height, updraft volume, and ice water path).

For FRPSs to be truly helpful to the lightning, atmospheric chemistry, and modeling communities, it is important to understand if there is variability in scheme performance by latitude zone, region, type of convection (e.g., airmass, multicell, and supercell), and time of year, and how schemes perform at different resolutions (e.g., cloud-resolved, regional, and global). To do this, thunderstorms from different environments and of differing updraft strength, size, and severity must be analyzed. In a study of storms over northern Alabama, Mecikalski and Carey (2017) showed that the altitude and reflectivity where flashes initiate and propagate vary as a function of storm type (i.e., multicells, mesoscale convective systems or MCSs, and supercells), thereby showing the importance of differentiating between various storm types when performing lightning-related studies. Barthe and Barth (2008) and Barthe et al. (2010) emphasize the need for modeling numerous convective case studies. Without understanding these variations, the true potential of the relationships between model storm parameters and total lightning activity will not be fully understood and the community will not be able to expand our knowledge of the impact of lightning in other areas (e.g., LNO_x, air quality, and climate). However, the effort described above would be quite large. The study we report in this paper for one storm system in one region can serve as a model for the more comprehensive analyses that are needed.

The objectives of this paper are to evaluate previously published and recently developed FRPSs in a cloud-resolved WRF model coupled with chemistry (WRF-Chem) simulation of the 29–30 May 2012 Oklahoma severe supercell system (Bela et al., 2016; Davenport et al., 2019; DiGangi et al., 2016; Li et al., 2017; Pollack et al., 2016) observed during the Deep Convective Clouds and Chemistry (DC3) field campaign (Barth et al., 2015) and determine which scheme best represents the observed flash rate trends and total number of flashes. Section 2 describes each FRPS investigated in the model simulation. Background on the DC3 field experiment and 29–30 May case study are provided in Section 3 and the model configuration is described in Section 4. The results from the model simulation and FRPS evaluation are presented in Sections 5 and 6, respectively, followed by a discussion of the FRPSs performance in Section 7. In Section 8, a summary of the case study results is provided.

2. Flash Rate Parameterization Schemes

Cloud-resolved models can incorporate explicit electrical schemes to study lightning activity in thunderstorms (e.g., Barthe et al., 2005; Fierro et al., 2013; Helsdon et al., 1992; MacGorman et al., 2001; Mansell et al., 2002). Bovalo et al. (2019) used total lightning from an explicit electrical scheme in eight different cloud-resolved Meso-NH model simulations and the model-simulated storm parameters to develop four FRPSs at both domain- and convective cell-scales. Schemes developed at the cell-scale performed better and were used to evaluate a storm observed during the Hydrological cycle in the Mediterranean Experiment. The simulation suggested that total graupel mass predicted total lightning well and that FRPSs with positive y-intercept values overestimate the total flash rate. The difficulties with using explicit schemes for simulating lightning flashes include the complexity of the electrical activity and the computational cost of modeling the intricate behavior (McCaul et al., 2009).

To avoid these difficulties, FRPSs based on storm parameter model output are a useful way to represent a thunderstorm's electrification. However, the schemes are only as good as the model's ability to predict the location and strength of the convection and the distribution of hydrometeors (Fierro et al., 2013). If the kinematic and microphysical characteristics are inaccurate, the non-inductive charging, which is believed to be the main mechanism for cloud electrification (Barthe et al., 2010; Jayaratne et al., 1983; Latham et al., 2007; Rakov, 2016; Saunders et al., 1991; Takahashi, 1978), will not be properly represented by the proxy parameters (e.g., updraft volume and graupel echo volume). This charging mechanism usually occurs where a strong updraft coincides with the mixed-phase region of the cloud (Deierling & Petersen, 2008; Deierling et al., 2008; Zipser & Lutz, 1994). Here graupel and ice crystals collide and rebound in the presence of supercooled liquid water and are transported by updrafts and downdrafts to achieve charge separation and eventually lightning initiation (Basarab et al., 2015; Deierling & Petersen, 2008; MacGorman & Rust, 1998; Saunders et al., 1991; Takahashi, 1978).

Yair et al. (2010) used the microphysics and vertical velocity fields from the cloud-resolved WRF model as a way to measure charge generation and separation and forecast lightning activity. This method, called the lightning potential index (LPI), was further developed by Lynn et al. (2012) into a lightning prediction algorithm, which considers the potential electric energy available for lightning production. Additional techniques are also incorporated into models to try to more precisely depict the evolution of the convective system and potentially improve the prediction of observed total lightning activity. Qian and Wang (2021) assimilated radar reflectivity data into the inner-most cloud-resolved domain of a nested WRF simulation of a MCS observed over China. Their results show that lightning flash rates less than or equal to 20 flashes 9 km^{-2} hr^{-1} are best represented by their FRPSs and specific filters that use the model graupel (i.e., graupel volume and precipitation ice mass (PIM)) and updraft volume (UV) storm parameters.

Since models do not perfectly replicate the features of an observed storm, a better representation of the observed flashes is produced using the regression between the observed and model-simulated storm parameters to adjust the FRPSs (Barthe et al., 2010) or by scaling the model-simulated flash rates. The research by Barthe et al. (2010) differs from previous work because it was the first time flash rate-storm parameter relationships developed from field experiment observations were tested in a cloud-resolved model. The performance of FRPSs in tropical island convection was also assessed for the first time by Cummings et al. (2013) using the WRF Aqueous Chemistry (WRF-AqChem; Barth et al., 2007) model to run a cloud-resolved simulation of a deep convective storm that occurred during the Stratospheric-Climate Links with Emphasis on the Upper Troposphere and Lower Stratosphere (SCOUT-O3)/Aerosol and Chemical Transport in Tropical Convection (ACTIVE) field campaigns near Darwin, Australia.

Table 1
Flash Rate Parameterization Schemes and Associated Required Criteria Thresholds Tested in the WRF-Chem Cloud-Resolved Simulation of 29–30 May 2012 Oklahoma Case Study

		Required criteria thresholds			
Flash rate parameterization scheme	Flash rate equation (reference)	Reflectivity (dBZ)	Temperature (°C)	Vertical velocity (m s^{-1})	Hydrometeor (g kg^{-1})
Maximum vertical velocity (w_{max})	$f = 5 \times 10^{-6} \times (w_{max})^{4.5}$ (Price & Rind, 1992)			Maximum	
Cloud top height (CTH)[a]	$f = 3.44 \times 10^{-5} \times CTH^{4.9}$ (Price & Rind, 1992)	>20	<0		
Updraft volume (UV)	$f = 6.75 \times 10^{-11} \times UV_5$ - 13.9 (Deierling & Petersen, 2008)		<−5	>5	
Ice water path (IWP)	FD = 33.33 × IWP - 0.17 (Petersen et al., 2005)	>25	<−10		
Precipitation ice mass (PIM)[b]	$f = 3.4 \times 10^{-8} \times PIM$ - 18.1 (Deierling et al., 2008)		<−5	w < vts	snow > 0.25 graupel > 0.5
Ice mass flux product (IMFP)[b]	$f = 9.0 \times 10^{-15} \times (f_p \times f_{np}) + 13.4$ (Deierling, 2006; Deierling et al., 2008)		<−5	Non-precipitation: w > vts; Precipitation: w < vts	ice > 0 snow > 0.25 graupel > 0.5
CSU graupel echo volume (CSU GEV)	$f = 7.0 \times 10^{-2} \times GEV$ (Basarab et al., 2015)	>35	−40 < T < −5		graupel > 0.5
CSU 35dBZ echo volume (CSU 35EV)	$f = 7.2 \times 10^{-2} \times 35EV$ (Basarab et al., 2015)	>35	−40 < T < −5		
CSU precipitation ice mass (CSU PIM)	$f = 1.2 \times 10^{-7} \times PIM$ (Basarab et al., 2015)	>35	−40 < T < −5		
UAH graupel echo volume (UAH GEV10)	f = 0.0534 × GEV10 (Carey et al., 2015)		−40 < T < −10		graupel > 0.5
UAH graupel echo volume (UAH GEV5)	f = 0.0430 × GEV5		−40 < T < −5		graupel > 0.5
UAH updraft volume (UAH UV)	f = 0.0337 × UV		−40 < T < −10	>5	
UAH graupel echo volume for supercells (UAH GEV10S)	f = 0.0674 × GEV10S		−40 < T < −10		graupel > 0.5
UAH graupel echo volume for supercells (UAH GEV5S)	f = 0.0569 × GEV5S		−40 < T < −5		graupel > 0.5
UAH updraft volume for supercells (UAH UVS)	f = 0.0403 × UVS		−40 < T < −10	>5	
Upward cloud ice flux (ICEFLUX)	$FD_l = 6.58 \times 10^{-7} \times$ ICEFLUX (Finney et al., 2014)			w > vts	ice > 0 snow > 0.25
OK 35dBZ echo volume (OK 35EV)	f = 0.0111 × 35EV + 1.6619	>35	−40 < T < −5		
Blended lightning threat (LTG3)	FD_{LTG3} = (0.95 × graupel flux) + (0.05 × VII) (McCaul et al., 2009, 2020)		T = −15		graupel > 0.5

Note. f is total flash rate in flashes min^{-1}, FD is flash density in flashes km^{-2} day^{-1}, FD_l is flash density over land in flashes $m_{grid\ cell}^{-2}$ s^{-1}, and FD_{LTG3} is flash density in flashes km^{-2} 5-min^{-1}. FRPS units and the storm parameters used within each flash rate equation are further defined in Section 2. [a]Indicates the highest altitude where both criteria are met. [b]Indicates the storm vertical velocity (w) and snow fall speed (vts) are both required.

Described below are 18 FRPSs for predicting total lightning. The schemes are evaluated in our study at a cloud-resolving scale and include those developed prior to and after the DC3 field experiment. The earliest FRPSs were based on kinematic and structural characteristics of thunderstorms, while more recent schemes evolved toward the use of microphysical variables. Table 1 lists each FRPS equation and the type of criteria threshold required by each scheme.

2.1. Cloud Top Height and Maximum Vertical Velocity

Early research investigated correlations between lightning flash rate and cloud top height (CTH) or maximum vertical velocity (w_{max}). Williams (1985) indicated a non-linear relationship existed between CTH and total lightning, as well as CTH and w_{max}, based on thunderstorms observed in New England, Florida, and New Mexico

(i.e., continental, midlatitude convection). Using these same data, Price and Rind (1992) further developed the relationships with the intent that they could be used at a coarse resolution to predict global lightning patterns. For use in cloud-resolved models, such as WRF-Chem, the CTH (km) is represented by the maximum height of the 20 dBZ radar reflectivity where the temperature is below freezing (0°C). Since updraft velocities play an important role in cloud electrification, Price and Rind (1992) used additional field measurements to investigate the differences in the relationships between w_{max} and CTH for thunderstorms over land and water. The results show there is a positive correlation between the two storm parameters and that when CTHs are similar, the w_{max} tends to be stronger for continental versus marine convection. This supported conclusions previously made by researchers regarding why lightning activity may vary given certain convective cloud characteristics. By combining the two equations, which link lightning flash rate (flashes min^{-1}) with CTH and CTH with w_{max}, a non-linear relationship between lightning activity and w_{max} (m s^{-1}) was defined. The horizontal resolution that is suggested as most appropriate for applying either FRPS is an area that is as wide as the storm is tall (Pickering et al., 1998; Williams, 1985).

2.2. Updraft Volume

The UV scheme (Deierling & Petersen, 2008) was developed on a storm scale using ground-based dual-polarimetric and dual-Doppler radar data and total lightning data from 11 convective events, which include single cell, multicell, and supercell thunderstorms. The events were observed in northern Alabama in 2005 and in Kansas and Colorado during the Stratospheric-Tropospheric Experiment: Radiation, Aerosols and Ozone (STERAO-A) and Severe Thunderstorm Electrification and Precipitation Study (STEPS) field campaigns. Total lightning data were provided by the Northern Alabama Lightning Mapping Array (LMA) and by the Office Nationale d'Etudes et de Recherches Aerospatiales (ONERA) lightning interferometer (in STERAO-A and STEPS). Deierling and Petersen (2008) indicate there is a strong correlation ($r = 0.93$) with total lightning when UV (m^3) is computed within the mixed-phase region (i.e., temperature < -5°C) where vertical velocities >5 m s^{-1} (UV_5). It is also suggested that this combination of criteria required for developing the scheme creates a robust relationship that is at least applicable in the two different regional environments in which the above thunderstorm events were observed. Negative flash rates are generated when $UV_5 < 2.06 \times 10^{11}$ m^3 because the linear relationship between UV and total lightning activity (flashes min^{-1}) has a non-zero y-intercept.

2.3. Ice Mass Flux Product and Precipitation Ice Mass

Ice mass flux product (IMFP) and PIM (Deierling, 2006; Deierling et al., 2008) are examples of flash rate-storm parameter relationships involving ice-phase hydrometeors. The IMFP and PIM schemes were both developed using the same thunderstorm cases and observed data as the UV scheme (Deierling & Petersen, 2008). The storm parameters were calculated at temperatures <-5°C, where PIM (kg) is a summation of only the graupel mass and IMFP (kg^2 m s^{-2}) involves the vertical motion of both the precipitation and nonprecipitation (suspended) ice masses through each grid point.

Hydrometeor types were derived from polarimetric radar data using fuzzy logic algorithms (Vivekanandan et al., 1999). The hydrometeor categories used by Deierling et al. (2008) to define precipitation ice included hail, hail/rain mixture, graupel/small hail/rain mix, and graupel/small hail. Nonprecipitation ice was classified as dry snow and ice crystals that were either irregular or horizontally oriented. Using the dominant hydrometeor identified at each radar grid point, Deierling et al. (2008) used the reflectivity (Z) - mass content (M) relationships to calculate the ice mass (Heymsfield & Miller, 1988; Heymsfield & Palmer, 1986). The precipitation ice mass flux (f_p; kg m s^{-1}) calculated by Deierling et al. (2008) used the precipitation ice terminal fall speed, while Barthe et al. (2010) indicated this could be replaced by the difference between vertical wind velocity and precipitating ice fall speed. Barthe et al. (2010) also suggested nonprecipitation ice mass flux (f_{np}; kg s^{-1}) may be determined using the difference between vertical wind velocity and nonprecipitation ice fall speed instead of horizontal divergence.

Both FRPSs indicate a linear relationship exists on a storm scale between the independent (IMFP or PIM) and dependent (total lightning activity) variables (Deierling et al., 2008). However, the y-intercepts are non-zero. This means lightning is produced (flashes min^{-1}) when IMFP is zero and negative flash rates occur when PIM $< 5.32 \times 10^8$ kg.

For our WRF-Chem simulation, precipitation ice includes graupel/hail and snow, while nonprecipitation ice includes snow and cloud ice. Precipitation (nonprecipitation) snow is considered to occur at model grid points

where the snow terminal fall speed determined by the microphysics scheme is greater (less) than the updraft velocity. Nonprecipitation ice is identified at model grid points where cloud ice exists and the vertical velocity >0 m s^{-1}. Model-simulated graupel/hail at any grid point is assumed to be precipitation.

2.4. Ice Water Path

The ice water path (IWP) scheme is another example of a FRPS based on hydrometeors and was developed using data from the Lightning Imaging Sensor (LIS) and Precipitation Radar instruments onboard the Tropical Rainfall Measuring Mission (TRMM) satellite during the 1998–2000 warm seasons (Petersen et al., 2005). Data points used in developing this relationship represent IWP (kg m^{-2}) and flash density (flashes km^{-2} day^{-1}) over 0.5° × 0.5° (~50 km × 50 km) grid cells between ±35° latitude. In our cloud-resolved model simulation IWP was calculated by integrating the precipitation and nonprecipitation ice mass at all points within a column where radar reflectivity >18 dBZ and temperature <−10°C (Barthe et al., 2010; Petersen et al., 2005). However, the column area is scaled down to the smaller WRF-Chem processor area (~18 km × 19 km) and the lightning flash density within the processor is converted to flash rate (flashes min^{-1}). While this scheme is linear, the *y*-intercept is negative. Therefore, a negative flash rate is generated when the IWP < 5.10×10^{-3} kg m^{-2}. The model-simulated hydrometeors included in the IWP storm parameter calculation are cloud ice, snow, and graupel/hail. Barthe et al. (2010) found that this FRPS scheme is sensitive to the radar reflectivity threshold used to evaluate the IWP. In their cloud-resolved simulation they adjusted for the overprediction in anvil reflectivity by increasing the reflectivity limit, so IWP is integrated over a smaller region. This caused IWP to increase for their simulated storm.

2.5. Upward Cloud Ice Flux

Developed from data over a similar area (±38° latitude) as the IWP scheme, the upward cloud ice flux (ICEFLUX; kg_{ice} m_{cloud}^{-2} s^{-1}) scheme defines a linear relationship using specific cloud ice content data (i.e., an estimate of suspended ice) from the ERA-Interim global atmospheric reanalysis provided by the ECMWF and lightning flash density data observed by LIS on 2.5° × 2.5° (~270 km × 250 km) grid cells (Finney et al., 2014). In our model the calculated flash density (flashes $m_{grid\ cell}^{-2}$ s^{-1}) was converted to flash rate (flashes min^{-1}) by accounting for the model domain's horizontal resolution. Our analysis represents the first time this scheme is evaluated at cloud-resolved resolution against individual storm observations and evolution. Finney et al. (2014) suggest ICEFLUX be evaluated at 440 hPa, since it is the cloud top pressure criterion for deep convective clouds specified by the International Satellite Cloud Climatology Project (ISCCP) (Rossow et al., 1996). Finney et al. (2014) also assessed this scheme at 440 ± 100 hPa to test its sensitivity to pressure. They found lower correlations at higher pressures and similar correlations at lower pressures, confirming that 440 hPa was a good choice. Romps (2019) chose to evaluate ICEFLUX along a fixed isotherm (260 K) that is close to the 440 hPa isobar to account for the charging layer and many other atmospheric properties that tend to follow isotherms versus isobars.

2.6. McCaul Lightning Threat Methods

Lightning threat methods developed by McCaul et al. (2009, 2020) forecast flash rate density (flashes km^{-2} 5-min^{-1}) using either graupel flux at −15°C or the gridded vertical ice integral (VII). The graupel flux is a product of the upward vertical velocity (m s^{-1}) and graupel mixing ratio (g kg^{-1}), while the VII focuses on the graupel, snow, and cloud ice mixing ratios (kg kg^{-1}) within the grid column. Seven convective events observed over northern Alabama were analyzed with WRF at cloud-resolved scales. Over the lifetime of each event, the maximum LMA flash origin density per 5-min and maximum model-simulated graupel flux or VII were identified within the domain and used to create linear relationships between lightning and ice hydrometeors. The slope of each line was then used to calibrate their respective equation. The graupel flux and VII methods capture the temporal variability and areal coverage of lightning activity, respectively, with a weighted summation of the two methods (0.95 graupel flux and 0.05 VII) providing the best prediction of flash rate density (McCaul et al., 2009). The weighted summation is referred to as the blended lightning threat (LTG3). Initially, the resulting flash rate densities determined by graupel flux and VII were only used when they exceeded a threshold of 0.01 and 0.40 flashes km^{-2} 5-min^{-1}, respectively. However, additional techniques were developed to address specific concerns. These include (a) increasing the graupel flux method threshold to 1.5 flashes km^{-2} 5-min^{-1} to handle winter stratiform weather, (b) forcing VII to have the same peak flash rate density as graupel flux to avoid divergence of

the individual lightning threat methods during high flash rate events, and (c) assigning a flash rate density threshold to the blended method for a more accurate depiction of areal coverage (McCaul et al., 2020). McCaul et al. (2020) investigated the sensitivity of their FRPS using 12 different combinations of microphysics and PBL schemes in WRF, including the Morrison 2-moment microphysics and YSU PBL schemes used in our case study.

2.7. Newly-Developed FRPSs From DC3

Observations from the DC3 field campaign were included in the creation of new total lightning-storm parameter relationships. Total lightning flash data collected by LMA and radar data within the northeast Colorado and northern Alabama DC3 study regions allowed for the development of additional FRPSs by Colorado State University (CSU) and the University of Alabama at Huntsville (UAH), respectively (Basarab et al., 2015; Carey et al., 2015). Data used in FRPS development for these regions were from the DC3 period as well as other years. Our study will evaluate the performance of these newly-developed schemes for the first time in a model at cloud-resolved resolution.

2.7.1. Colorado FRPSs

Nine of the 11 isolated storms (i.e., single cell and supercell with varying severity) used by Basarab et al. (2015) in developing new FRPSs were from DC3, while the other two events were from summer 2013. All events were objectively identified using a cell-tracking algorithm (Fuchs et al., 2015). The average and maximum total flash rates associated with the observed convection data set are 53.9 and 287.8 flashes min^{-1}, respectively. In addition to LMA data, the polarimetric radar data were gridded at $0.5 \times 0.5 \times 0.5$ km^3 resolution and fuzzy logic algorithms (Dolan et al., 2013) were applied to the radar data to identify the dominant hydrometeor type per grid. Basarab et al. (2015) used the isolated Colorado convective events data set to modify previously developed FRPSs from the literature (e.g., PIM; kg). These schemes were not properly tuned to capture the higher flash rate Colorado storms and were also developed using a different hydrometeor identification algorithm.

In addition, graupel echo volume (CSU GEV; km^3) and 35 dBZ echo volume (CSU 35EV; km^3), which are similar to PIM and have previously shown strong correlations to lightning (Carey & Rutledge, 1996; Liu et al., 2012; Wiens et al., 2005), were also used to develop FRPSs for Colorado storms. To calculate the storm parameters, data points were restricted to the mixed-phase region of convective clouds (i.e., $-5°C >$ temperature $> -40°C$ and reflectivity > 35 dBZ). The linear relationships between the CSU PIM, GEV, and 35EV and total lightning resulted in a better fit to the data than the prior existing schemes in the literature. The CSU 35EV was the most successful storm parameter for estimating total lightning flash rates in Colorado. Basarab et al. (2015) also suggest this scheme may be robust enough to be used in different environments and regions based on its exceptional performance when used to examine thousands of isolated convective events from four areas (i.e., Colorado, Oklahoma, northern Alabama, and Washington, D.C.). This scheme performed best when the environment had low normalized convective available potential energy (NCAPE < 0.1 m s^{-2}), moderate warm cloud depth (1–2 km), and moderate vertical wind shear (10–20 m s^{-1}).

2.7.2. Northern Alabama FRPSs

Carey et al. (2015) developed FRPSs using 32 convective cells observed over northern Alabama, which ranged in storm type and severity (i.e., multicell, supercell and one quasi-linear convective system). Five of the events occurred during DC3. Unlike the CSU approach, which used a cell-tracking algorithm to identify and track isolated convective cells (Fuchs et al., 2015), UAH (Carey et al., 2015) used both objective and subjective approaches for tracking. The manual approach was necessary for the multicell events observed during DC3 to avoid any influence from nearby storms. Based on the LMA data, this data set had an average total flash rate of 12.5 flashes min^{-1} and a maximum of 102 flashes min^{-1}. Polarimetric and Doppler radar data were also available and fuzzy logic algorithms were utilized to determine the dominant hydrometeor types (Vivekanandan et al., 1999). Both data sets were gridded at 1 km resolution in the horizontal and vertical. Of the 17 storm parameters tested for the northern Alabama region, the linear relationships between total lightning (flashes min^{-1}) and graupel echo volume between $-10°C >$ temperature $> -40°C$ (UAH GEV10; km^3) (Carey et al., 2015), graupel echo volume between $-5°C >$ temperature $> -40°C$ (UAH GEV5; km^3), and updraft volume between $-10°C >$ temperature $> -40°C$ and vertical velocities >5 m s^{-1} (UAH UV; km^3) appeared to best handle both the normalized median and mean bias errors. Given these storm parameters, three additional FRPSs were developed using the

methods described by Carey et al. (2015) and the eight supercell events observed over northern Alabama (UAH GEV10S, GEV5S, and UVS).

2.7.3. Tailored FRPS for 29–30 May 2012 Convective Event

Since the objective of our study was to evaluate FRPSs in a simulation of an Oklahoma thunderstorm observed during DC3, it was desirable to include a scheme based on data from this region. According to Basarab et al. (2015), the 35EV was the most robust storm parameter used in their analysis for estimating lightning flash rates given how well it performed when tested using thousands of isolated storms in multiple regions of the continental United States. Therefore, CSU developed a version of this scheme using data from the Weather Surveillance Radar-1988 Doppler (WSR-88D) at Oklahoma City (KTLX) and the Oklahoma LMA during the 29–30 May 2012 event. The observed 35EV (km^3) and total lightning flash rates (flashes min^{-1}) resulted in a linear relationship based on convection located north of Oklahoma City (35.49°N). This Oklahoma 35EV (OK 35EV) scheme applied the same mixed-phase region temperature criteria as the CSU 35EV scheme (−5°C > temperature > −40°C). A similar relationship was found in two cells within a MCS observed in Oklahoma during the Thunderstorm Electrification and Lightning Experiment (TELEX) in 2004, where lightning initiation typically occurred within the 35 dBZ reflectivity contour in the presence of graupel (Lund et al., 2009).

3. Deep Convective Clouds and Chemistry (DC3) Experiment

The May–June 2012 DC3 field campaign provided a multi-faceted approach to study varying types of convection (e.g., midlatitude airmass, multicell, and supercell thunderstorms), their convective transport of trace gases (e.g., anthropogenic, biogenic, and wildfire emissions), and associated lightning occurrence and NO_x production, particularly with the FRPSs defined in Table 1. Field experiments prior to DC3 did not use as extensive an array of ground-based and airborne measurements of thunderstorms as DC3 to investigate the influence of the environment and convection on the composition and chemistry of the upper troposphere. Nor did previous campaigns combine these observations with those taken of the environment prior to and during convection, and with the outflow downwind 12–48 hr post-convection.

The operations center was located in Salina, Kansas, which offered reasonable flight times for research aircraft to arrive at any of the three pre-determined sampling regions in northeast Colorado, central Oklahoma to west Texas, and northern Alabama. The three domains were selected based on the available instrumentation and type of convection associated with the region. Additional details regarding the DC3 field campaign may be found in Barth et al. (2015).

3.1. The 29–30 May 2012 Oklahoma Severe Supercell System

On 29 May 2012 conditions were very unstable and favorable for convective development within the Oklahoma domain. The morning sounding from Norman, Oklahoma, showed the wind profile generally had a westerly component with veering from the surface to 600 hPa. A dryline was located across the Texas panhandle and a cold front stretched across the Ohio River Valley from northeast-to-southwest, with the southern portion pushing northward as a warm front over Oklahoma and Kansas. By 21:10 UTC the front was quasi-stationary and two isolated cells developed to its south along the Kansas-Oklahoma border and ahead of the dryline. The convection is in a similar location at 21:50 UTC. Over the next several hours both supercellular storms formed mid-level mesocyclones (DiGangi et al., 2016) and subsequently evolved into a line of supercells. The supercell line continued in an east-southeast direction, and new, non-supercellular storm cells formed both behind the supercell line and far downstream within the merged forward anvil region of the supercells (DiGangi et al., 2021). The combined anvil-initiated storm line and remnant supercells subsequently coevolved to form an MCS that moved through central Oklahoma during the period 03:00–04:00 UTC on 30 May.

Meteorological data collected by ground-based instrumentation in the Oklahoma domain include radar data from the NSSL WSR-88D or Next Generation Radar (NEXRAD) located near Norman, Oklahoma, and the NOAA/NSSL X-band polarimetric (NOXP) and C-band Shared Mobile Atmospheric Research and Teaching (SMART) radars. Lightning data are provided by the National Lightning Detection Network (NLDN) and the central Oklahoma Lightning Mapping Array (LMA) network (Bruning, 2014). The NLDN CG flash detection efficiency is ∼95% over the continental United States (Holle et al., 2014; Nag et al., 2011). The total lightning flash detection efficiency provided by the 11 stations in the LMA network is >90% at a 200 km radius (Chmielewski &

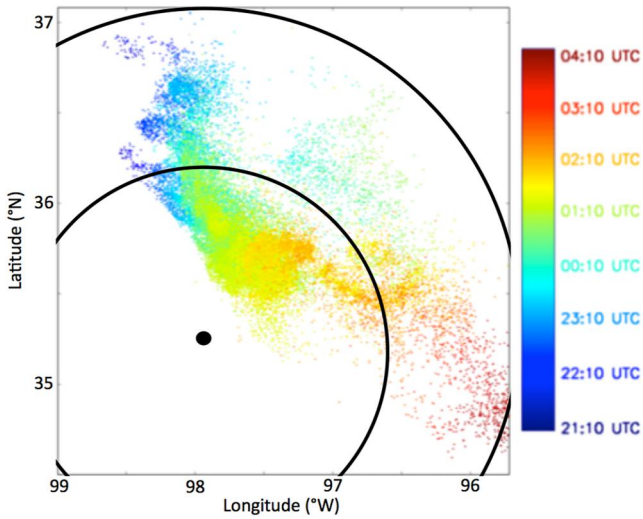

Figure 1. Location and time (colors) of each flash initiation point observed by the central Oklahoma LMA network from 21:10 UTC on 29 May to 04:19 UTC on 30 May 2012. The 3- and 2-D lightning detection coverage is represented by the 100 and 200 km radius from the center of the network, respectively. The network center is located at approximately 35.279°N, 97.918°W.

Bruning, 2016). The convection developed north of the LMA network within its 2-D lightning detection coverage (Figure 1). As the storm system progressed east-southeastward, it stayed within the 2-D coverage of the network for most of its life (21:10–04:19 UTC) and the majority of flashes were within the 3-D coverage between 23:40 and 03:00 UTC.

The NSSL Mobile GPS Advanced Upper-Air Sounding System (MGAUS) provided upper air data in the far-inflow region of the storm. Three mobile soundings were deployed at 20:29 UTC (35.667°N, 98.341°W) and 22:55 UTC (35.854°N, 98.066°W) on 29 May and 00:21 UTC (35.595°N, 97.859° W) on 30 May (Ziegler, 2013a). Visible satellite imagery from the Geostationary Operational Environmental Satellite-13 (GOES-13) was used to estimate the anvil area of the observed storm system from 21:10 to 01:00 UTC, prior to reduction in sunlight and the quality of the visible images (NCAR, 2012b).

The observed total lightning flash rate time series was generated from a grid of LMA data with 1-min temporal and 1-km spatial resolution. Figure 2a shows that the maximum flash rate observed by the LMA occurred at 01:37 UTC (312 flashes min^{-1}). The CG flash rate time series was produced from the observed NLDN flash data with weak positive CG flashes (peak current < +15 kA) filtered out. The peak CG flash rate (94 flashes min^{-1}; Figure 2a) occurred roughly 15 min later (01:51 UTC). Approximately 8,679 CG and 31,633 total flashes were observed over the lifetime of the convection with an average total flash rate of 75.5 flashes min^{-1}. Roughly 15,060 total flashes occurred during the initial 5-hr period simulated in our case study (20:00–01:00 UTC observed time), with an average total flash rate of 68.5 total

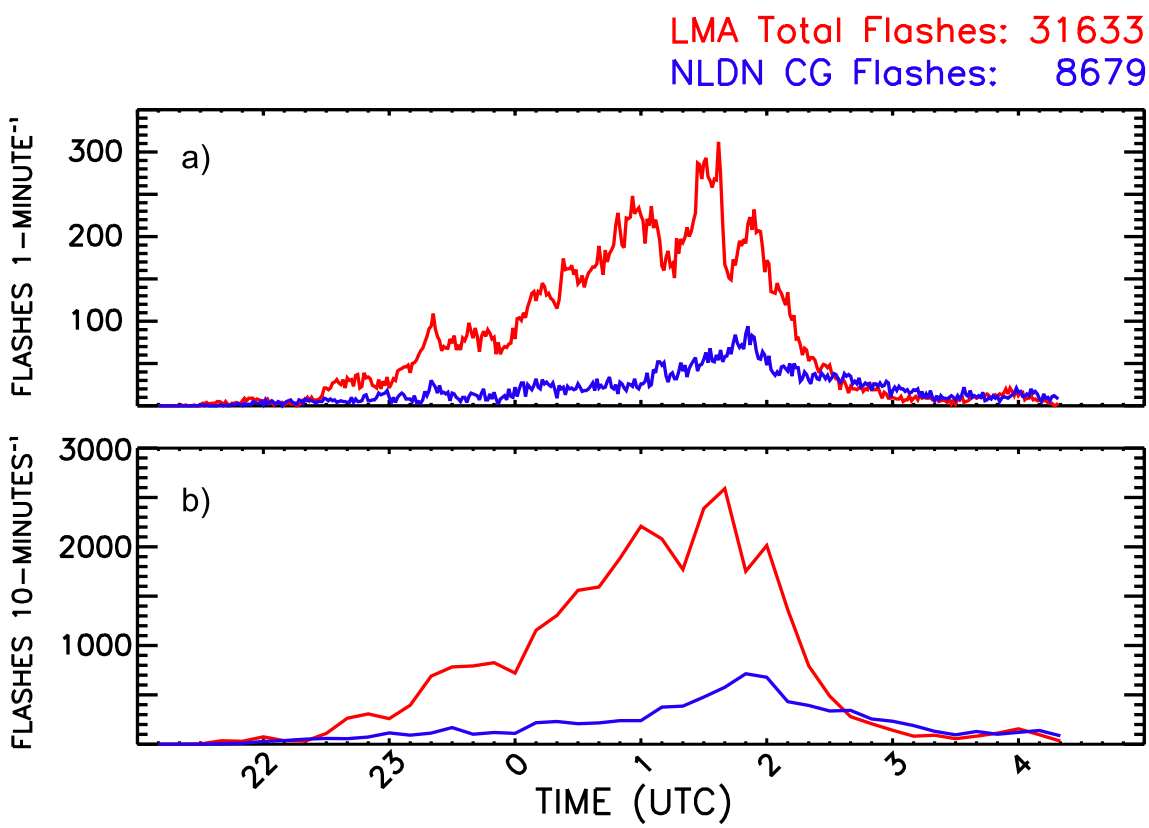

Figure 2. The Oklahoma LMA total and NLDN CG lightning flash data per (a) 1-min and (b) 10-min provided for the lifetime of the observed 29–30 May 2012 severe supercell system (21:10–04:19 UTC).

flashes min^{-1}. The 1-min data from both networks were binned into 10-min intervals (Figure 2b) to match the output from the WRF-Chem model. The total flash rate time series shows several distinct peaks as the flash rate increased from 21:30 UTC to the maximum (~2,600 flashes 10-min^{-1}) at 01:40 UTC. These peaks occurred at 22:00 UTC, 22:50 UTC, 23:50 UTC, and 01:00 UTC with roughly 100, 300, 800, and 2,200 total flashes 10-min^{-1}, respectively. Following the primary peak, the observed flash rate decreased at a faster rate than it increased. DiGangi et al. (2021) documented the distinct total and cloud-to-ground flashes began within the anvil-initiated storms far to the east of the Kingfisher storm, which was within the southern portion of the convection analyzed in this case study. The 29–30 May 2012 convection contained high flash rate supercells with small flash extents (Barth et al., 2015). DiGangi et al. (2016) also showed that the Kingfisher storm had an abundance of small flashes, especially during its mature phase, when flash rates were >100 flashes min^{-1}.

4. Methodology

4.1. Model

Bela et al. (2016) simulated the 29–30 May supercell system at cloud-resolved resolution using the WRF-Chem model, version 3.6.1. We use the same model conditions as Bela et al. (2016), but with some modifications, which are outlined below, to improve the similarity between the modeled and the observed storm properties. The model domain contains 480 × 420 × 89 grid points in the x, y, and z directions with 1-km horizontal resolution and variable vertical resolution from 50 m near the surface to 250 m at the top of the domain (50 hPa). The southwest corner of the domain is located at 33.8196°N, −99.7726°W and the northeast corner is located at 38.1354°N, −95.0998°W. Our simulation ran with chemistry turned off (i.e., chem_opt = 0) while we identified which FRPS best represents the observed lightning for follow-on WRF-Chem analyses. The initial 8-hr simulation ran from 18:00 UTC on 29 May to 02:00 UTC on 30 May using 480 processors on the NCAR Yellowstone supercomputer. The simulation did not extend past 02:00 UTC because we were interested in this time period for atmospheric chemistry analyses when lightning would be influencing the NO_x mixing ratios sampled by the DC3 aircraft in the anvil outflow (Pickering et al., 2024). For subsequent simulations a restart file was used at 21:00 UTC to reduce computation time since the observed convection began just after 21:00 UTC. The simulation was integrated with a 3-s time step, while the lightning parameterization was called every 6 s. Meteorological initial and boundary conditions were provided by the 6-hr interval North American Mesoscale Analysis (NAM-ANL). However, after an initial screening analysis of all 18 FRPSs, longer-duration simulations were desired for the six best performing schemes. These runs used the same model set up, but were extended to 06:00 UTC. The 12-hr simulation ran on the NCAR Cheyenne supercomputer because it replaced Yellowstone.

The initial model configuration and physics options were based on Bela et al. (2016). The Morrison 2-moment microphysics scheme predicts the mass mixing ratio for cloud droplets, and both mass and number mixing ratios for rain, cloud ice, snow, and graupel/hail (Morrison et al., 2015). The dense precipitating ice options can influence the storm structure, cold pool, and precipitation of deep convection due to differences in their terminal fall speed and bulk density (Adams-Selin et al., 2013; Bryan & Morrison, 2012; Morrison & Milbrandt, 2011; van Weverberg, 2013). For severe continental deep convection, such as the 29–30 May case study, we set the dense precipitating ice to have hail characteristics. Table 2 provides the final model physics options selected for this analysis.

The equations for all FRPSs, except the ICEFLUX and LTG3 schemes, were calculated per computer processor within the model domain using a single or summed storm parameter value. Each processor was roughly 18 km × 19 km in area and likely contained partial storm cores as the simulated storm moves through the domain. This approach could overestimate total lightning flashes for the linear schemes with positive y-intercepts, as well as non-linear schemes. Flash rates may also be underestimated by linear schemes with negative y-intercepts. For the ICEFLUX and LTG3 schemes, their methodologies appeared to indicate the calculations were performed per grid cell; therefore, the equations were also applied per grid cell within each processor in our model simulation.

In addition, the linear FRPSs with non-zero y-intercepts were only used when the storm parameter calculated for the processor exceeded a specific minimum value. This prevented negative flash rates, which are not realistic, from occurring in the UV, IWP, and PIM schemes and positive flash rates from occurring when the IMFP value was zero.

Table 2
WRF-Chem Model Physics Options Selected for 29–30 May 2012 Oklahoma Case Study

WRF-Chem model physics options	Name of scheme
Microphysics	Morrison 2-moment scheme
Planetary boundary layer	Yonsei University (YSU) scheme
Surface layer	MM5 similarity scheme
Land surface	Unified Noah land-surface model
Radiation (shortwave & longwave)	Rapid radiative transfer model for GCMs (RRTMG) scheme
Cumulus parameterization	None
Lightning flash rate parameterization	18 schemes (see Table 1)
Convective damping	Li et al. (2017)
Lightning data assimilation (LDA)	Fierro et al. (2012, 2014, 2015)

4.2. Convective Damping and Lightning Data Assimilation Techniques

Methods can be used to guide the model when simulations do not reproduce the observed convection in the correct space or time. The convective damping technique first clears convection from the model prior to the observed convective initiation by reducing the model-simulated water vapor at each 3-D grid point where relative humidity exceeds a specific threshold (Li et al., 2017). In our case study, water vapor was constrained to be less than a relative humidity of 75% from 21:00 to 21:30 UTC (prior to the beginning of continuous observed lightning flashes at 21:31 UTC) in order to decrease excessive buoyancy.

Water vapor is then reintroduced using a lightning data assimilation (LDA) technique (Fierro et al., 2012, 2014, 2015), so buoyancy is generated at the proper times and locations for convective development. Their equation is:

$$Q_v = AQ_{sat} + BQ_{sat}\tan(CX)\left[1 - \tanh\left(DQ_g^{2.2}\right)\right], \quad (1)$$

where Q_v is the water vapor mixing ratio (g kg^{-1}), Q_{sat} is the water vapor saturated mixing ratio (g kg^{-1}), Q_g is the graupel mixing ratio (g kg^{-1}), X is the flash rate, and constant coefficients are represented by A, B, C, and D. For this case study, the coefficient values are 0.93, 0.20, 0.01, and 0.25, respectively. Coefficient A controls the minimum threshold for relative humidity within a grid column to ensure the relative humidity stays above a predefined minimum value (93%). The default value for coefficient A is 0.81, but can be increased for weakly electrified storms (Fierro et al., 2012). While this case study is considered a high flash rate event, coefficient A was varied between 0.81 and 0.95. A value of 0.93 provided a closer representation of the observed storm when used in combination with the convective damping and other LDA variables.

Previous studies have added water vapor back into the column within the mixed-phase graupel-rich region (0°C to −20°C) (Fierro et al., 2012, 2014, 2015), the lower troposphere (<700 mb) (Fierro et al., 2016; Marchand & Fuelberg, 2014), and between the lifting condensation level (LCL) and w_{max} height (Li et al., 2017). Our focus was on improving the mixing ratio and vertical placement of the simulated hydrometeors (e.g., graupel), so water vapor was introduced between the LCL (16°C) and the lower level of the mixed-phase region (−5°C). If this lower limit was extended to colder temperatures, it is possible the water vapor may instantly deposit onto ice particles and not provide the desired improvement.

The lightning stroke counts detected by the Earth Network Total Lightning Networks (ENTLN) from 21:30 to 23:00 UTC (i.e., roughly the beginning of the continuous lightning to the mature stage) were gridded using the same 1 km × 1 km horizontal resolution as the WRF-Chem and introduced into the model over the same time period. At model grid points with more than one stroke, graupel mixing ratios <3.0 g kg^{-1}, and ambient relative humidity <95%, the LDA modified the water vapor between −5 and 16°C. The relative humidity was also constrained to be ≤103%.

5. Evaluation of Model-Simulated Convection

Prior to inclusion of the convective damping and LDA techniques, WRF-Chem represented the observed storm location, dimensions, and vertical motion reasonably well; however, the model-simulated anvil area was ∼60%–95% smaller than the observations during the first hour and roughly 20%–50% smaller after that time. The majority of the FRPSs also grossly overestimated the LMA flash rates observed in the 29–30 May severe supercell system. Every hydrometeor-based scheme overpredicted, which prompted an investigation of the model-simulated hydrometeor mixing ratios and their location within the convection.

The damping and LDA methods were tested with the intent of improving the location and mixing ratio of the hydrometeors in the model. By removing excess moisture from the atmosphere in locations with no observed convection and then guiding water vapor back into the atmosphere with the help of lightning observations, the maximum graupel mixing ratio decreased by ∼2 g kg^{-1} and the height of the maximum lowered by ∼1 km. While these methods have provided the best results thus far for modifying the hydrometeors in this case study, the remaining errors in the WRF-Chem hydrometeors are likely due to microphysics scheme assumptions. The simulation results in Section 5.1 are based on the model's final configuration, which includes damping and LDA (Table 2).

In addition to incorporating the damping and LDA, several other approaches were used to explore the overprediction. These included assigning thresholds to the frozen hydrometeors and scaling the model hydrometeors to an approximation of the actual hydrometeors. Each approach is described in Section 5.2. The NSSL 2-moment microphysics scheme (Mansell et al., 2010) was also tested using the LDA assumptions of Bela et al. (2016) and the damping and LDA assumptions in this study; however, both simulations yielded a poorer representation of the storm system. Because the NSSL cloud microphysics did not represent the storm well, additional simulations using the WRF-ELEC model (Fierro et al., 2013; Mansell et al., 2010) containing this microphysics scheme would not benefit our goal of determining a FRPS that can be used with atmospheric chemistry simulations of the 29–30 May storm.

5.1. Meteorological Conditions

The observed and model-simulated storms both began along the Kansas-Oklahoma border. The first model-simulated storm began at 22:10 UTC, approximately an hour after the observed convection initiation (CI), and subsequently evolved within a highly sheared and thermodynamically unstable local storm environment (Figure 3). The model simulation reasonably reproduced the observed storm-environmental profiles of wind, temperature, and humidity (Figure 3). However, the temporal offset between similar observed and simulated storms subsequently decreased to about 30–50 min as the simulated storms matured. Figures 4 and 5 show the location of the observed (left column) and simulated (right column) cells at the observed and model times at which the spatial agreement is best. Figures 4a and 4b show the location of the observed and simulated linearly arranged supercells 40 min after their respective CI events. As the supercells formed a north-south line, both the observations (Figure 4e) and model (Figure 4f) indicate radar reflectivities of 60–65 dBZ in similar locations. Subsequent discussion will assume a 40-min (±10 min) time difference between the later simulated and earlier observed features of the storms and their near-inflow environments unless explicitly noted otherwise.

As new, non-supercellular storm cells developed beneath the far eastern downstream anvil to the east of the supercell line (Figure 5a), and subsequently evolved to form an MCS (DiGangi et al., 2021), they were not resolved by the WRF-Chem simulation (Figure 5b). It is noteworthy that DiGangi et al. (2021) identified the "Findeisen-Knight" process as likely having forced the secondary anvil storms, via snow sublimative cooling into dry, mid-tropospheric sub-anvil air that subsequently forced a surface-based downdraft, adjacent mesoscale updrafts, and sub-anvil CI in the adjacent updrafts. While the observations show an orientation of the supercell line toward the southeast, the model tilts the line toward the southwest by the end of the simulation. However, both the NEXRAD (Figure 5c) and model (Figure 5d) indicate that the southernmost cell in the main system (i.e., the "Kingfisher storm") is most dominant.

The WRF-Chem simulation captures several additional aspects of the severe supercell system: (a) the east-southeast progression of the line and the cells that form to its west, (b) the development of the "Kingfisher storm" and its merger with the northern cell, and (c) the initiation and northeast motion of the cell to the south (weaker and slower-moving than observed) that merges with the convective system, although later than observed.

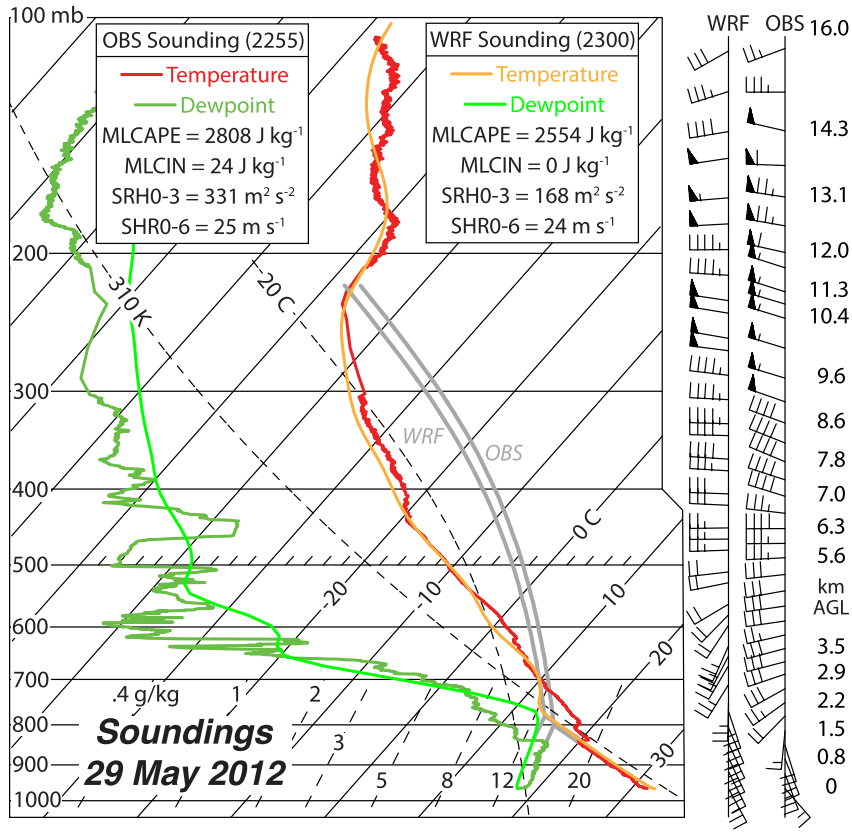

Figure 3. The NSSL MGAUS ("OBS") and WRF-Chem model-simulated ("WRF") skew-t sounding diagrams on 29 May 2012. The NSSL MGAUS released from (35.854°N, 98.066°W) at 22:55 UTC is a composite of the 22:55 UTC sounding below 435 mb with the 20:29 UTC sounding above 435 mb, as justified by weak upper-tropospheric evolution, the need to fill missing OBS upper-level values to compute conserved lifted parcel thermodynamic properties (DiGangi et al., 2021), and agreement with the overlaid WRF sounding. The WRF sounding represents 23:00 UTC model time at the same location as the observed sounding. Legends list OBS and WRF sounding parameters and denote colors of the respective temperature and dewpoint profiles. Sounding parameters include mixed-layer convective available potential energy (MLCAPE), mixed-layer convective inhibition (MLCIN), 0–3 km storm-relative helicity (SRH0-3), and 0–6 km bulk shear (SHR0-6). A half wind barb = 2.5 m s^{-1}, a full barb = 5 m s^{-1}, and a pennant = 25 m s^{-1}. Height is in km above ground level (AGL).

However, the convection to the northwest and southwest of the line of supercells is slightly delayed in the model. A comparison between the observed visible satellite imagery and the model-simulated total hydrometeors from 22:10 to 01:00 UTC model time suggests the model-simulated storm underestimates the anvil area by ∼60%–70% for the initial 30–40 min of development and is within 10% after that time. The eastern edge of the anvil begins to move outside the model domain after 01:00 UTC; therefore, no further comparisons of anvil size were made.

The model-simulated composite radar reflectivity indicated that the size of the convective cores was similar to the storm observed by NEXRAD, both in the horizontal and vertical. Generally the convective regions (>30 dBZ) had dimensions of 20–40 km in the east-west and 20–30 km in the north-south directions for both the observed and model-simulated storms. However, the model has difficulty maintaining the individualized areas of higher reflectivity that are noted in the NEXRAD composite reflectivity. While the LDA was being applied, the convective cells in the simulated storm appeared more individualized, as in the observations. After the LDA stopped, it became more difficult to discern individual cells as the areas of simulated higher reflectivity appeared to merge. The maximum radar reflectivity simulated by the model (∼69 dBZ) was within the range of the observations (65–70 dBZ). The average height of the model-simulated storm, based on the 10 dBZ contour in Figures 4 and 5, was within roughly −9% to 17% of the observed 10 dBZ contour. Unlike the observations, radar reflectivities >50 dBZ tend not to extend above 9 km altitude in the model (Figure 6).

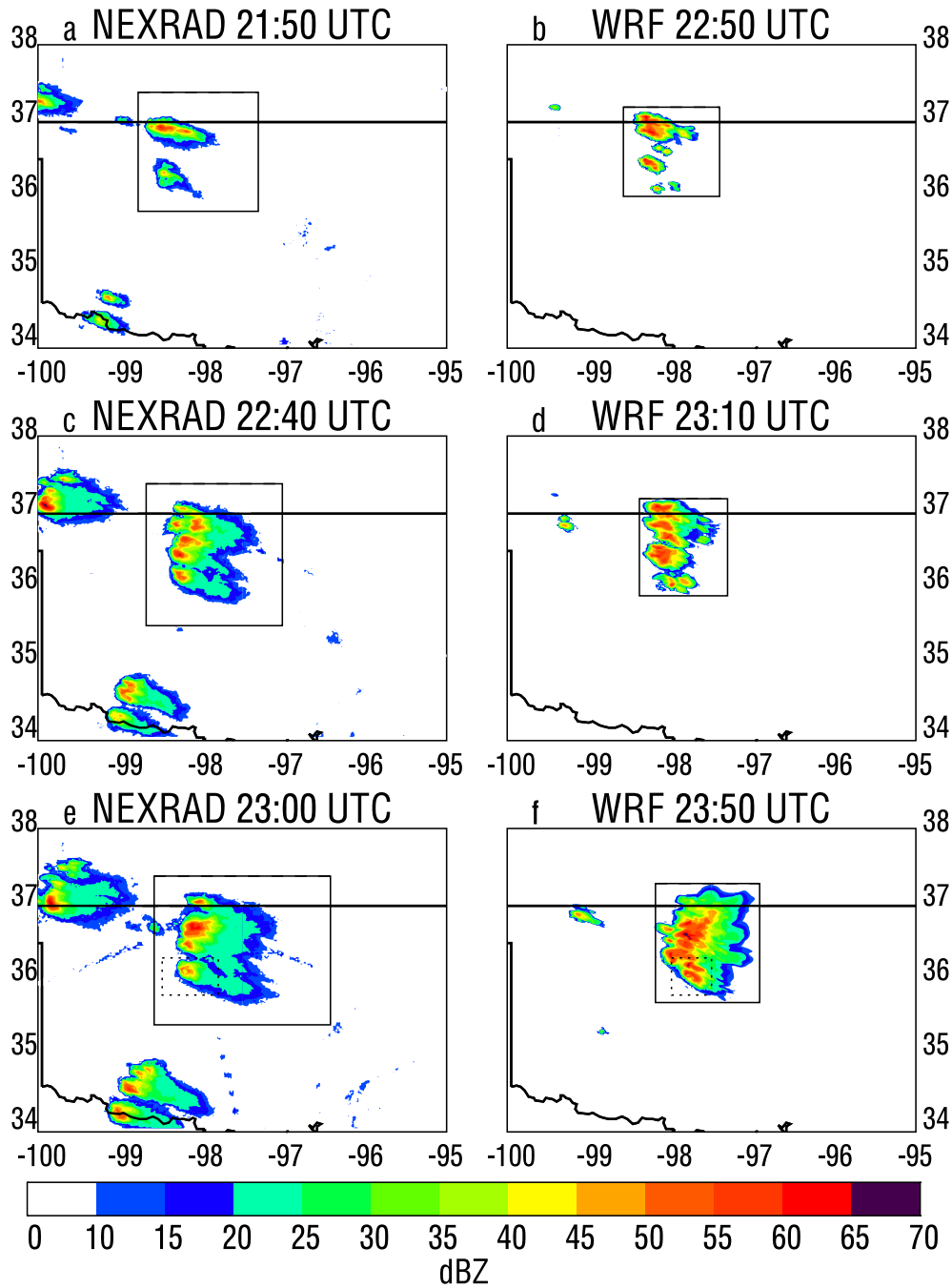

Figure 4. Composite radar reflectivity from the 29–30 May 2012 severe supercell system for the observed storm at (a) 21:50 UTC, (c) 22:40 UTC, and (e) 23:00 UTC observed time, and the WRF-Chem model-simulated storm with damping and LDA techniques at (b) 22:50 UTC, (d) 23:10 UTC, and (f) 23:50 UTC model time. Note, there is a 1-hr delay in the model-simulated storm initiation, but this offset is not maintained as the storm matures. The black box in each image highlights the portion of the convection that is the focus of the observations and model-simulation at the selected time. The dotted black box in (e) and (f) represents the location of the Kingfisher storm.

Since six FRPSs rely on radar reflectivity to compute storm parameters, the observed and model-simulated radar volumes are compared at times when similar features were noted. Just after storm initiation, the simulated 18, 25, and 35 dBZ echo volumes greatly overestimated the observations before decreasing 30 min later to an over-estimation of about 7%, 15%, and 45%, respectively (Figures 4a and 4b). As the model-simulated storm evolved,

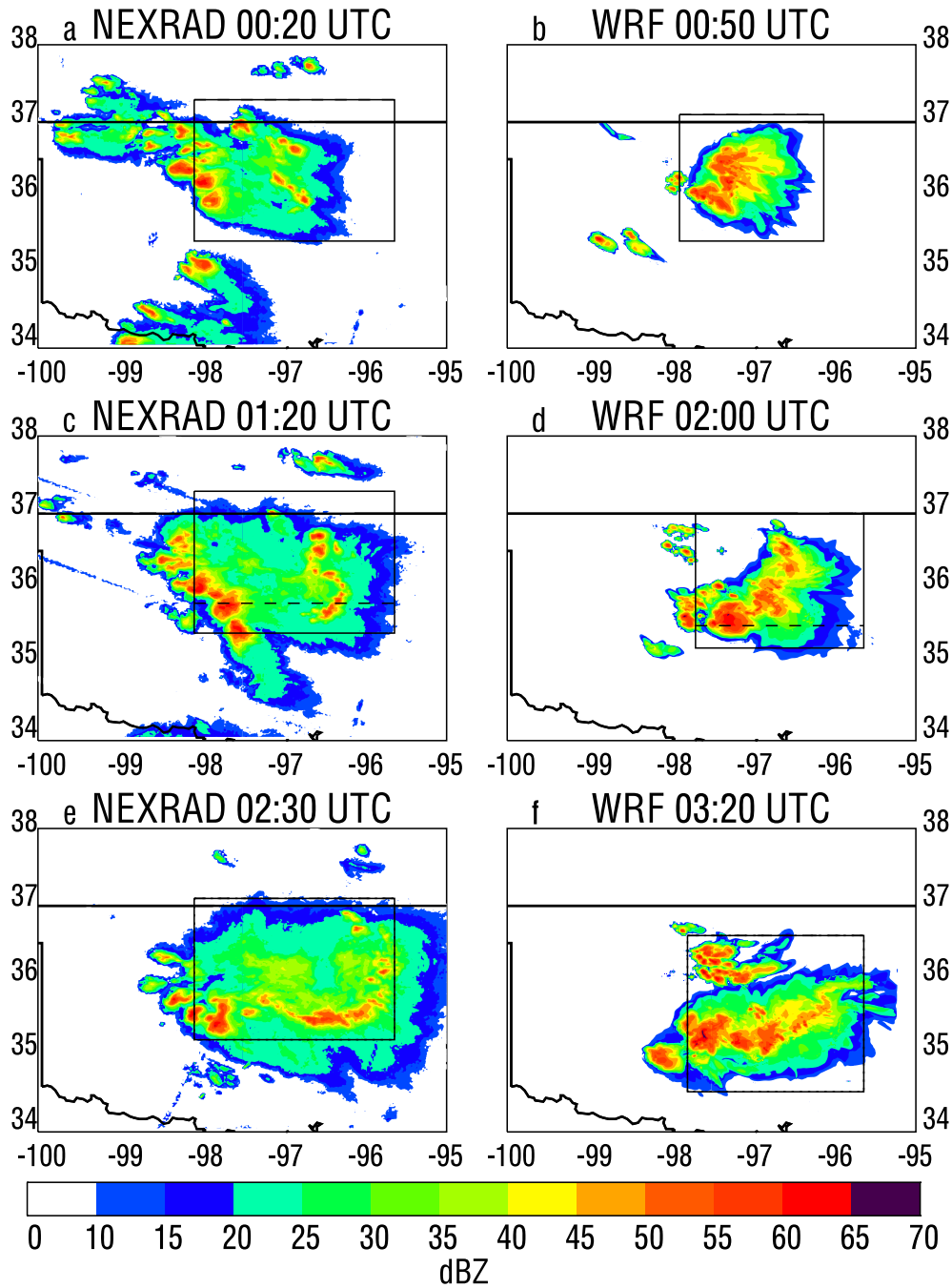

Figure 5. Same as Figure 4, except for the observed storm at (a) 00:20 UTC, (c) 01:20 UTC, and (e) 02:30 UTC observed time, and the WRF-Chem model-simulated storm with damping and LDA techniques at (b) 00:50 UTC, (d) 02:00 UTC, and (f) 03:20 UTC model time. The black dashed line in (c) and (d) represents the location of the vertical cross section in Figure 6.

the 18 and 25 dBZ echo volumes generally underestimated the observations by roughly 32%–44% and 13%–25%, respectively, (Figures 4c, 4d, and 5a–5d) except for a ∼9% and ∼49% overestimation about 2–2.5 hr after initiation (Figures 4e and 4f). This implies the observed stratiform region tends to be under represented by the model. The simulated 35 dBZ echo volume mostly overestimated the observations by ∼11%–59% (Figures 4c–4f and 5a, 5b), but was within −2% of the observations about 4 hr after the storm began (Figures 5c and 5d). This suggests the model storm was initially too intense given the large overestimation of the 35 dBZ volume, but generally became more similar to the observations as the storm matured.

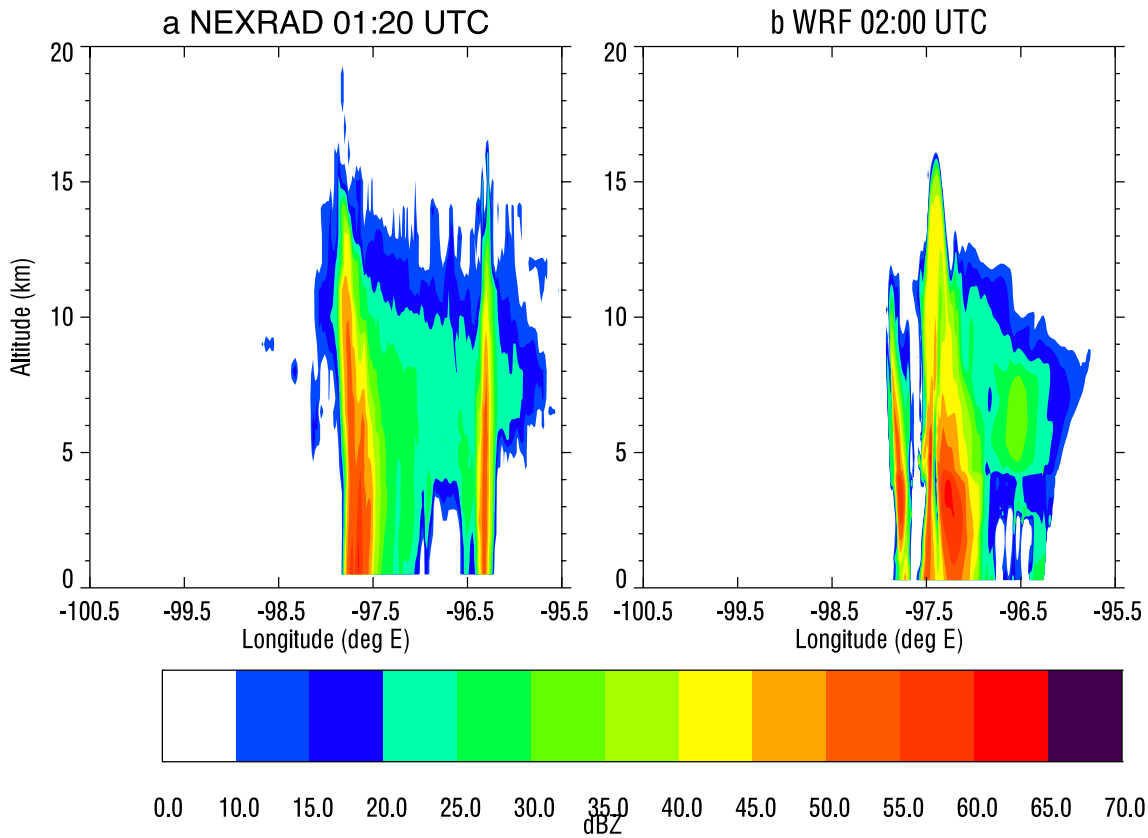

Figure 6. Vertical cross-section of radar reflectivity from the 29–30 May 2012 severe supercell system for the (a) observed storm at 01:20 UTC observed time and 35.8° N and (b) WRF-Chem model-simulated storm with damping and LDA techniques at 02:00 UTC model time and 35.5°N.

The WRF-Chem model generates a storm in an environment with a mixed-layer convective available potential energy (MLCAPE) of 2,554 J kg^{-1}. This is similar to the 22:55 UTC observed mobile sounding (2,808 J kg^{-1}), although the simulated upper air profile is slightly more moist in the upper troposphere and has a slightly deeper boundary layer (Figure 3). Similar to the observed sounding, the simulated profile indicates veering in the lower troposphere with upper-level winds with a westerly component, along with a surface-6 km bulk shear (24 m s^{-1}) that is comparable to the observations (25 m s^{-1}). The model-simulated convection generated a maximum vertical velocity (~62 m s^{-1}) within ~5% of the mobile radars observations (~65 m s^{-1}) (DiGangi et al., 2016). The observed and simulated maximum values both occurred in the southernmost cell of the system at the same time relative to storm initiation (23:30 UTC observed time and 00:30 UTC model time), but the maximum was located at 8–9.5 km altitude in the observations (Bela et al., 2016) and at ~10 km altitude in the simulation.

5.2. Hydrometeors

5.2.1. Proxy Observations

Hydrometeors play a key role in the FRPSs that are tested in WRF-Chem, with 10 of the 18 schemes directly involving relationships between total lightning activity and hydrometeors and three schemes involving calculated radar reflectivity, which depends on the hydrometeors. Before the current damping and LDA techniques were applied, the model-simulated flash trends based on hydrometeors were overpredicting the observed total lightning. DiGangi (2014) and DiGangi et al. (2016) investigated the hydrometeors in the Kingfisher storm using a diabatic Lagrangian analysis (DLA) retrieval approach every 3 min from 22:51 to 00:00 UTC observed time. The DLA, a thermal-microphysical continuity retrieval that is constrained by the observed 4-dimensional radar wind and reflectivity fields, is implemented via a simple Lagrangian cloud model (Chmielewski et al., 2020; DiGangi et al., 2016; Ziegler, 2013b, 2013c). Subject to simplified microphysics in the DLA that is compensated for via

accurate Lagrangian transport combined with derivation of precipitation contents directly from the 4-D radar reflectivity field, the DLA's retrieved hydrometeor fields are assumed to be a reasonably close approximation of the actual hydrometeor contents (e.g., Waugh et al., 2018). If our WRF-Chem simulation closely captures the hydrometeors of the Kingfisher storm on the southern end of the simulated supercell line, then it is presumed that the northern supercells will also be represented to the same degree.

Horizontal and vertical hydrometeor cross-sections through the model-simulated southern convection (00:00–00:40 UTC model time), prior to the current damping and LDA assumptions, were compared against the DLA hydrometeor mixing ratios provided by DiGangi (2014) and DiGangi et al. (2016) from 23:20 to 00:00 UTC observed time, following the ∼40-min temporal offset discussed in Section 5.1. These proxy observations are provided at three to five altitude levels ranging from 1.2 to 12.2 km for graupel/hail, 6.2–16.2 km for snow/ice, and 4.7–7.2 km for rain water and cloud water at each of three times. The specific altitudes of the radar-derived horizontal cross-sections are identified in DiGangi (2014). Subject to the acknowledged differences between radar-observed and simulated storms and the contrasting microphysical parameterizations employed by the WRF-Chem model and the DLA, a comparison of the maximum WRF-Chem and DLA hydrometeor concentrations averaged over all of the available altitudes of the Kingfisher storm during the 40-min period indicated that WRF-Chem overestimated the maximum DLA graupel mixing ratios by roughly 25% while underestimating the snow/ice by roughly 20%. Since WRF-Chem underestimates cloud water by less than 10% relative to the DLA, it is considered similar to the proxy observations below 7.2 km. Rain water, however, is overestimated by ∼70% below 7.2 km from the WRF-Chem relative to the DLA. Bela et al. (2016) compared the simulated precipitation (rain and graupel) from their WRF-Chem run against the mean hourly precipitation from the NCEP Stage IV analysis. Their comparison suggested that although there were differences in the precipitation distribution, the observed total precipitation received at the surface was overestimated by <20% in the northern convection from 23:40 to 00:40 UTC model time.

5.2.2. Ice Hydrometeor Thresholds

Initially the FRPSs requiring graupel and snow used mixing ratio thresholds of 1.0×10^{-12} g kg^{-1}. This was believed to be too low and a possible cause for the overestimation by the hydrometeor-based FRPSs (not shown), as these thresholds would potentially include grid cells outside the charging region (e.g., stratiform anvil precipitation region). For the final model set-up the minimum graupel and snow mixing ratio thresholds were increased to 0.5 and 0.25 g kg^{-1}, respectively, to better represent the kinematic and microphysical processes related to charging in the convective core. Raising both thresholds helped to reduce the total flashes (e.g., in the CSU GEV scheme the estimated total flashes were reduced by ∼20%). However, the LMA observations were still overestimated by the hydrometeor-based schemes.

Given the results from Section 5.2.1, several attempts were made to reduce the graupel/hail and increase the snow within the convection by modifying the Morrison 2-moment microphysics scheme. The threshold for converting snow to graupel/hail by riming was increased, which should decrease the amount of graupel/hail within the cloud. The results (not shown) indicate that increasing the snow threshold from 0.1 to 0.5 g kg^{-1} or 1.0 g kg^{-1} led to a 1%–10% and 2%–50% decrease in the model-simulated graupel/hail and snow/ice concentrations, respectively. Therefore, this modification was not applied because it did not significantly reduce the amount of graupel/hail present in the 29–30 May model-simulated storm and it also decreased the amount of snow when an increase was needed.

5.2.3. Scaling Hydrometeor Mixing Ratios

The vertical cross sections of model hydrometeors from the WRF-Chem simulation with damping and LDA (Figure 7) also show the model-simulated graupel, snow, and ice do not extend over the same altitude ranges as indicated by the proxy observations. Rain water was not investigated in more detail because it was assumed to be precipitating and not contributing to the overestimation of the hydrometeor-based FRPSs. Therefore, a closer inspection was undertaken of the vertical distribution of WRF-Chem frozen hydrometeors and these hydrometeors were compared with those from the DLA. The analysis suggests the graupel overestimation is primarily above 9 km altitude and the snow/ice underestimation mainly occurs between 11 and 13 km altitude. By focusing on these specific altitudes for the three times during the 40-min period, instead of all altitudes, it was determined that WRF-Chem (a) overestimated graupel by roughly 55% above 9 km altitude, (b) overestimated

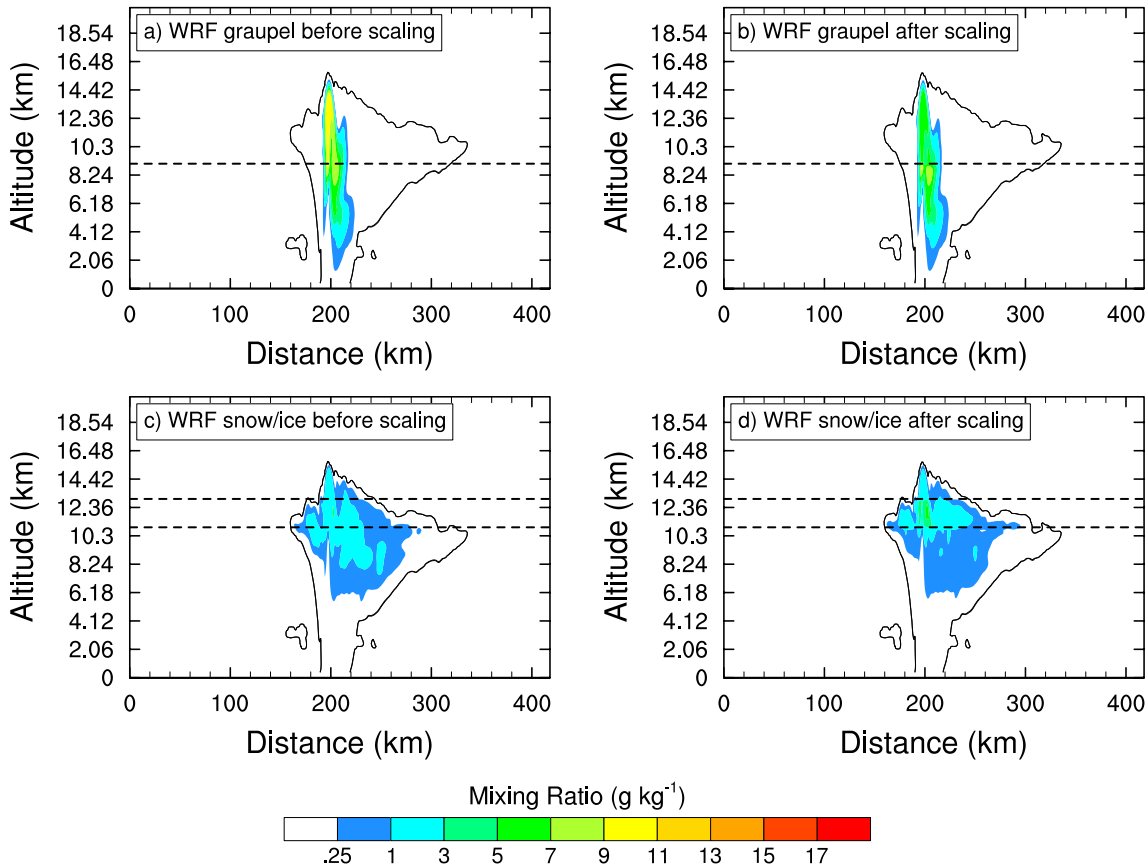

Figure 7. The WRF-Chem model-simulated graupel (top) and snow/ice (bottom) mixing ratios at 00:20 UTC model time and 36.0°N before (a, c) and after (b, d) the altitude-specific scaling factors are applied to the hydrometeors in the FRPS code only. The solid black line represents the outline of the cloud, where total hydrometeors equal 0.01 g kg^{-1}. The dashed black lines indicate the specific altitudes where the scaling factors are applied. In the top figures, a graupel scaling factor is only applied above 9 km. In the bottom figures, a different snow/ice scaling factor is applied below 11 km and between 11 and 13 km.

snow/ice by 31% below 11 km altitude, and (c) underestimated snow/ice by 42% between 11 and 13 km altitude. Altitude-specific scaling factors for the hydrometeors were developed based on these percentage biases.

Figure 7 uses vertical cross sections through the approximate location of the Kingfisher storm in the southern portion of the WRF-Chem model-simulated convection to compare the graupel and snow/ice mixing ratios before and after the altitude-specific scaling factors are applied to the hydrometeors in the WRF-Chem output. The results show the altitudes of maximum mixing ratio of the model-simulated graupel and snow/ice are more representative of the proxy observations after scaling is applied. For example, at 23:40 UTC observed time DiGangi (2014) indicated that above the freezing layer the maximum observed graupel/hail mixing ratio is ~9.0 g kg^{-1} between 8.2 and 8.7 km. Prior to scaling the WRF-Chem-simulated graupel/hail, the largest mixing ratios (9–10.8 g kg^{-1}) at the corresponding model time (00:20 UTC) are located between ~8.3 and 14.4 km (Figure 7a). After applying the scaling factors (Figure 7b) the maximum mixing ratios are similar (9–10.2 g kg^{-1}), but found over a smaller altitude range (~8.5–9 km) that is closer to the observed height. For the proxy observed snow/ice, the maximum mixing ratio (8–10 g kg^{-1}) is between 11.7 and 13.2 km (DiGangi, 2014; DiGangi et al., 2016). The maximum WRF-Chem-simulated snow/ice mixing ratio increases from 3.1 g kg^{-1} between 11.3 and 12.5 km (Figure 7c) to 5.3 g kg^{-1} within a similar altitude range (11–13 km) after scaling (Figure 7d). While the WRF-Chem-simulated snow/ice is still underestimating the proxy observations at this time and vertical cross-section location, the horizontal distance covered by the simulated snow/ice mixing ratios (1–5 g kg^{-1}) has slightly increased within this altitude layer.

With the application of the current damping and LDA assumptions, the location and maximum mixing ratio of the model-simulated hydrometeors were adjusted closer to the observations. These techniques did not correct the

Table 3
Number of Model-Simulated Total Lightning Flashes Predicted From 22:10 to 02:00 UTC Model Time by the 18 Flash Rate Parameterization Schemes Before and After the Model-Simulated Hydrometeors Are Scaled Within the Schemes

	Model-simulated lightning flashes		
Flash rate parameterization scheme	No scaling	Scaling	Percent change (%)
w_{max}	134,870	134,791	−0.1
CTH	31,264	31,547	+0.9
UV	29,147	29,151	+0.0
IWP	175,589	157,787[a]	−10.1
PIM	143,918	116,949	−18.7
IMFP	1,087,677	971,504	−10.7
CSU GEV	108,250	99,455	−8.1
CSU 35EV	156,896	110,818	−29.4
CSU PIM	192,513	116,908	−39.3
UAH GEV10	102,534	99,853	−2.6
UAH GEV5	95,302	93,138	−2.3
UAH UV	16,096	16,089	−0.0
UAH GEV10S	129,417	126,030	−2.6
UAH GEV5S	126,109	123,246	−2.3
UAH UVS	19,249	19,240	−0.0
ICEFLUX	13,698	9,938[b]	−27.5
OK 35EV	24,783	23,488	−5.2
LTG3	57,376	57,350	−0.1

Note. Results are from simulations that include damping and LDA. The LMA observed 15,060 total lightning flashes from 21:10 to 01:00 UTC. [a]When IWP is evaluated at 25 dBZ, the number of total lightning flashes is 143,743 (−18.1%). [b]When ICEFLUX is evaluated at 390 hPa, the number of total lightning flashes is 14,419 (+5.3%).

hydrometeors perfectly, so scaling to the DLA proxy observations was required to improve the simulated hydrometeors for our case study. However, some discrepancies still exist after scaling (i.e., graupel is slightly overestimated and snow/ice is slightly underestimated). For use in the WRF-Chem simulation, the altitude-specific scaling factors are only applied to the hydrometeors in the FRPS code, not in the microphysics scheme.

6. Performance Evaluation of Lightning Prediction Schemes

6.1. Initial Evaluation of Schemes

We initially examine the flash rate time series and total flashes predicted by all 18 FRPSs over the simulation period ending at 02:00 UTC model time and compare them with the LMA observations. The lightning included in the analysis occurs within the bounding boxes that are manually adjusted every 10-min to envelop the simulated and observed convection as the system matures. Examples of the location of these boxes are provided in Figures 4 and 5. We assume that the "flash" described in a FRPS can be compared to the LMA observations for this convective event as long as the FRPS flashes are represented by flash rate in flashes min^{-1} over an area that is similar to that of the model processor. The schemes are evaluated against the observations and each other starting at the moment when reflectivity is first noted in the NEXRAD (21:10 UTC) and the model (22:10 UTC). As indicated by the reflectivity analysis, the time evolution of the observed and model storms differ, which may affect the flash rate comparisons. The number of total flash counts generated by each FRPS before and after scaling the hydrometeors is provided in Table 3. This shows the overestimation of the flash rates and total flashes persists for the five non-hydrometeor-based schemes and 12 of the 13 hydrometeor-based schemes. The remainder of this section presents the results from the WRF-Chem simulations with LDA, damping, and hydrometeor scaling based on the proxy observations.

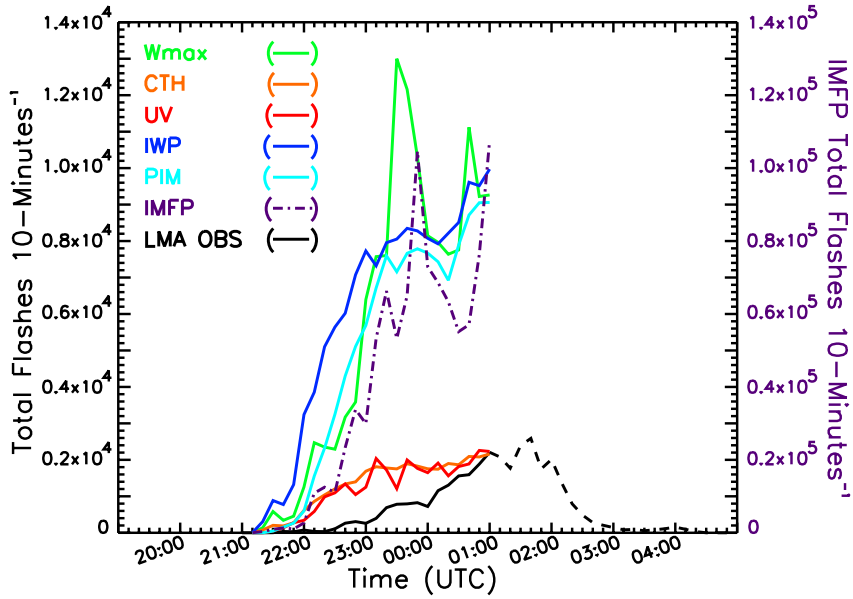

Figure 8. The total lightning flash rates per 10-min from the LMA (black) and the FRPSs based on relationships between storm parameters and total lightning activity from the literature. The *y*-axis on the right-hand side of the plot is scaled up by one order of magnitude to represent the flash rates based on IMFP. The model-simulated lightning flash rates are based on a WRF-Chem run with damping/LDA techniques, and hydrometeor altitude-specific scaling factors are applied to the FRPS code only. The FRPSs represent the model-simulated trends from 22:10 to 02:00 UTC model time, but each time series is adjusted 60 min earlier to coincide with the observed storm initiation time (21:10 UTC). The solid black line represents the observed lightning flashes from 21:10 to 01:00 UTC, which covers the same time period as the simulated flashes. The dashed black line represents the continuation of the observed time series after 01:00 UTC.

Figure 8 shows the observed and model-simulated flash rate time series for the six schemes analyzed by Barthe et al. (2010), while Figures 10 and 11 show the time series for the remaining 12 FRPSs. Literature indicates that several FRPSs are sensitive to their application criteria. IWP involves a radar reflectivity threshold of 18 dBZ; however, if the model-simulated reflectivity produces higher values than observed, the threshold should be increased to better represent the IWP (Barthe et al., 2010). For a supercellular system that produced 72,068 flashes over northern Alabama, Mecikalski and Carey (2017) found the LMA sources peaked between 7 and 9 km altitude and between 20 and 25 dBZ; although the majority of the sources from the system occurred between 4 and 13 km and between 15 and 55 dBZ. The LMA sources in our case study are generally located between 6.5 and 11.5 km within the 20–55 dBZ reflectivity contours and maximize at 9 km between 25 and 30 dBZ (Figure 9). Therefore, the threshold used in the scheme is increased to 25 dBZ to better represent the electrified portion of the storm and reduce the overestimation. While this helps decrease the total flashes by 9% for this scheme, the overprediction is still a factor of 9.5, as indicated in Table 3 and Figure 8.

Figure 10 focuses on the three CSU-developed schemes (Basarab et al., 2015), the ICEFLUX scheme (Finney et al., 2014), the LTG3 scheme (McCaul et al., 2009, 2020) and the scheme developed with the 29–30 May data. Figure 11 displays results from the FRPSs developed by UAH (Carey et al., 2015; and Table 1).

ICEFLUX is sensitive to the pressure level at which the scheme is evaluated (Finney et al., 2014), as well as which hydrometeors are classified as suspended ice crystals. Finney et al. (2014) developed this scheme using the specific cloud ice water content variable from the ERA-Interim reanalysis, which includes graupel, snow, and ice. To mimic this variable with WRF-Chem, the mixing ratios of the three hydrometeors were summed and only included graupel and snow if their fall speeds were less than the updraft velocity. Upon initial evaluation the results showed ICEFLUX overestimates the LMA total lightning flashes by roughly a factor of 4. However, if graupel is considered to be precipitating (i.e., not suspended), then ICEFLUX underestimates (9,938) the observations (15,060) (Table 3).

The 440 hPa pressure level used by ICEFLUX is the ISCCP cloud top pressure threshold for deep convective clouds (Rossow et al., 1996). However, 440 hPa is found at the very lowest location of cloud ice in our model-

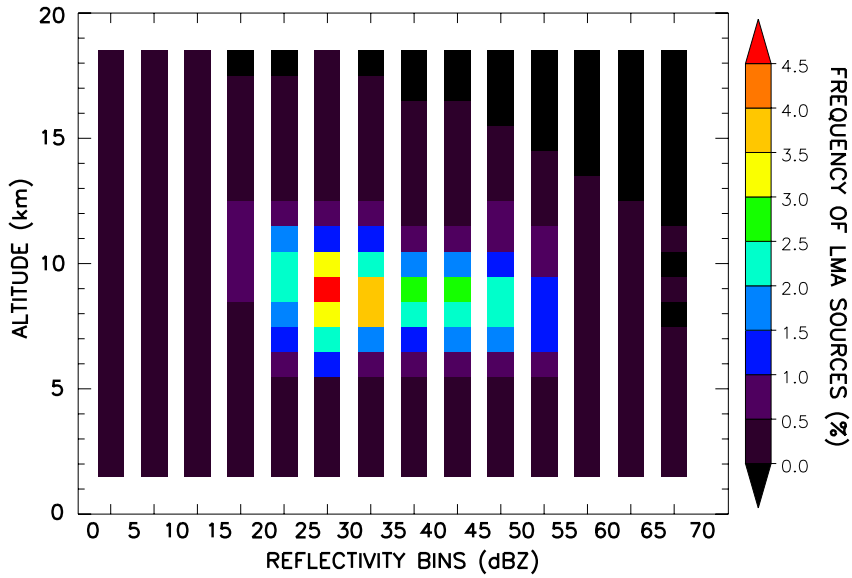

Figure 9. Percentage of the very high frequency (VHF) sources observed by the central Oklahoma LMA from the 29–30 May 2012 severe supercell system (21:10–04:19 UTC) by altitude and reflectivity.

simulated storm. If we evaluate the scheme at 340 hPa, as tested by Finney et al. (2014), the underestimation becomes an overestimation (19,216). Therefore, a 100 hPa decrease in pressure (i.e., 440 to 340 hPa) resulted in a 10,000 total flash increase. If the ICEFLUX pressure level is adjusted by 50 hPa (390 hPa) instead, then the total number of model-simulated flashes (14,419) is within ∼4.3% of the observations (15,060), as shown in Table 3. For the remainder of this case study, all analyses involving ICEFLUX are evaluated at 390 hPa to better represent the storm.

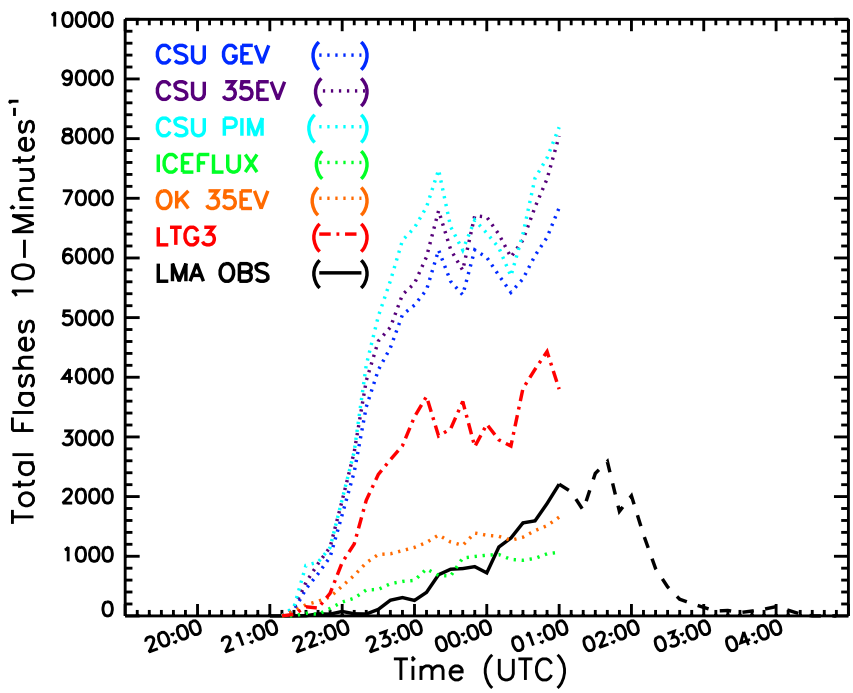

Figure 10. Same as Figure 8, except the FRPSs are based on relationships between storm parameters and total lightning activity developed by CSU (Basarab et al., 2015), Finney et al. (2014), and McCaul et al. (2009, 2020).

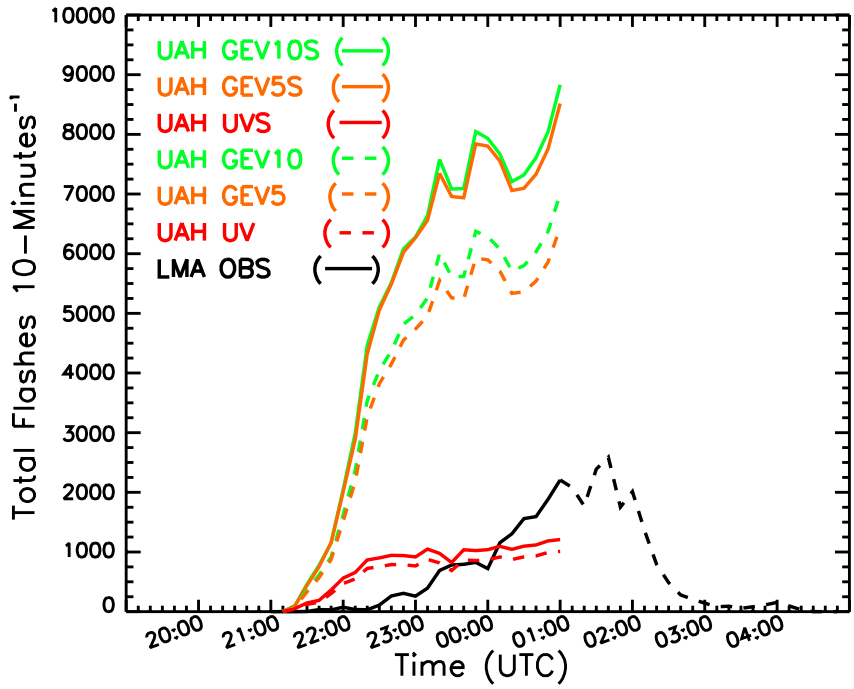

Figure 11. Same as Figure 8, except the FRPSs are based on relationships between storm parameters and total lightning activity developed by UAH (Carey et al., 2015).

On average the non-hydrometeor-based FRPSs overestimated the number of LMA total flashes by a factor of 3, while the hydrometeor-based schemes overpredicted by a factor of 11. IMFP has the largest difference between the model-simulated and observed total flashes (a factor of >60). If the IMFP scheme is excluded, the observations are overestimated on average by a factor of 7 by the remaining hydrometeor-based schemes.

For all FRPSs, the total flash counts increase earlier in the model storm than in the observed storm. The initial peak in the observed flashes (~100 flashes 10-min^{-1}) occurs 50 min after convective initiation, while seven of the 18 schemes (CTH, ICEFLUX, IMFP, IWP, CSU PIM, LTG3, and w_{max}) predict peaks of varying magnitudes (~50–1,400 flashes 10-min^{-1}) roughly 20 min after the model storm develops (Figures 7 and 9).

An interesting feature that appears in most of the FRPS trends is a change in the steepness of the flash rate slope just after 22:00 UTC observed time (23:00 UTC model time). While the trends are generally steeper than the observations within the first few hours of storm initiation, the model trend becomes slightly smaller after the first hour. In both UAH UV schemes (Figure 11), this change results in a slightly flatter slope than the other schemes that also exhibit this feature. The timing of this feature coincides with the end of the LDA and its modification of the water vapor in the atmosphere. For the w_{max}, IMFP, PIM, LTG3, and ICEFLUX schemes, this transition is not apparent in the trends. This suggests that the storm parameters used in these five FRPSs use variables and criteria thresholds that are not influenced by the LDA to the same degree as the other schemes.

The model flash rate time series for the IWP and PIM schemes (Figure 8) have peaks that coincide with the observed peaks at 23:50 UTC observed time. The four UAH GEV (Figure 11) and three CSU (GEV, 35EV, PIM) (Figure 10) schemes show multiple peaks between 23:00 and 00:00 UTC, instead of one like the observations and the IWP and PIM schemes; however, these schemes are similar because there is no prolonged increase in the flash rates during this time. The UV scheme hints at the presence of the peaks at 22:50 UTC and 23:50 UTC, although the trend is fluctuating at these times. The two schemes that appear to replicate the timing and general shape of the observed peaks fairly well from 21:30 to 00:30 UTC, but not the magnitude, are those based on IMFP and w_{max} (Figure 8). ICEFLUX behaves similarly, but the peak at 22:50 UTC is not as distinct as it is in the observed, IMFP, and w_{max} flash rate trends, plus it occurs ~30 min earlier. Generally, when the flash rate peaked in a scheme, the time offset from the observations was consistent with the storm evolution noted in the radar reflectivity.

Table 4
Centered Root Mean Square Error of the Model-Simulated Total Lightning Flashes per 10-min (Left) and Mean Bias in the Model-Simulated Total Lightning Flashes per 10-min (Right) Predicted From 22:10 to 02:00 UTC Model Time (21:10–01:00 UTC Observed Time)

Flash rate parameterization scheme	Centered root mean square error (flashes)	Flash rate parameterization scheme	Mean bias (flashes)
ICEFLUX	411	ICEFLUX	−27
OK 35EV	426	UAH UV	43
UV	458	UAH UVS	174
CTH	460	OK 35EV	351
UAH UVS	484	UV	587
UAH UV	500	CTH	687
LTG3	1,019	LTG3	1,762
UAH GEV5	1,731	UAH GEV5	3,253
CSU GEV	1,835	CSU GEV	3,516
UAH GEV10	1,881	UAH GEV10	3,533
CSU 35EV	2,061	CSU 35EV	3,990
CSU PIM	2,208	CSU PIM	4,244
UAH GEV5S	2,418	PIM	4,245
UAH GEV10S	2,483	UAH GEV5S	4,508
IWP	2,750	UAH GEV10S	4,624
PIM	2,846	w_{max}	4,989
w_{max}	3,728	IWP	5,362
IMFP	33,494	IMFP	39,852

Note. The LMA flashes used in the calculation are from 21:10 to 01:00 UTC observed time and the ICEFLUX parameter is evaluated at 390 hPa.

Prior to this study a FRPS had not been developed for Oklahoma convection. Since 35EV was considered a robust storm parameter given its performance in regions outside of Colorado, the FRPS was tailored for Oklahoma using observations from our 29–30 May case study. However, when the scheme was employed in WRF-Chem, the total number of observed lightning flashes was still overestimated (~56%; Table 3). Figure 10 also shows the detailed features of the observed flash rate trend are missing, which is likely due to the high-bias in storm intensity during convective initiation. This is noticed by the large overestimation of the 35 dBZ echo volume (~500%) in the initial cells that develop at the start of the simulations both with and without LDA. After roughly 1-hr, the overprediction by the 35 dBZ echo volume becomes smaller (~30%) before turning into a slight underestimation (~15%). The increased intensity during the developing stage of the storm system may help explain why the predicted flash rates for this scheme, and others, lack some of the details seen in the observed flash rate trend (i.e., the observed peak at 22:50 UTC).

An additional technique used the mean bias between the observed and model-simulated flashes per 10-min to evaluate the performance of the FRPSs. The schemes were ranked based on their root mean square error after the mean bias between the observed and simulated flashes was removed (i.e., centered root mean square error) and based on their mean bias (Table 4). For this case study, both calculations identified the same six FRPSs (i.e., ICEFLUX, OK 35EV, the three UV schemes, and CTH) as being the best at predicting flash rate fluctuations and total flashes over the 21:10–01:00 UTC period, and selected the same lowest ranked scheme (i.e., IMFP).

In terms of biases and the total flashes predicted over the simulation, the best performing FRPSs include ICE-FLUX (Finney et al., 2014) (which is similar to the LMA total lightning flashes during roughly the first 4 hr of convection), the three UV schemes developed by Deierling et al. (2008) and UAH (Carey et al., 2015) (i.e., all convection types and supercell-only in northern Alabama), the OK 35EV scheme, and the CTH scheme (Price & Rind, 1992).

However, when the model-simulated flash rates are not adjusted an hour earlier to coincide with the start time of the observed storm, then the initial trend in the model flash rate time series appears to better represent the

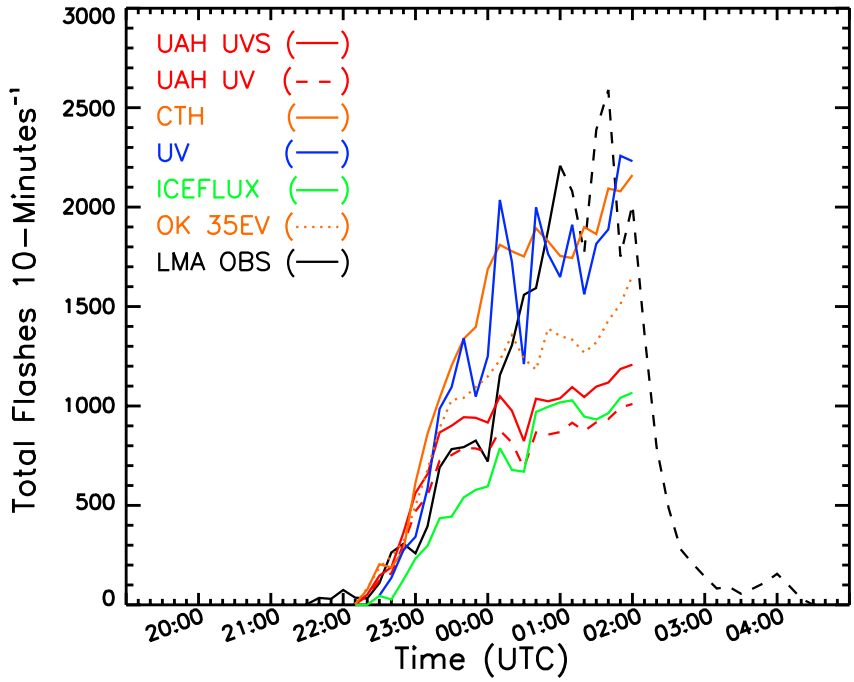

Figure 12. Same as Figure 8, except the FRPSs are based on relationships between storm parameters and total lightning activity with an overall total lightning flash count most similar to the Oklahoma LMA observations for the 21:10–01:00 UTC period. The model-simulated flash rate time series are not adjusted earlier to coincide with the observed storm initiation time and instead are plotted from 22:10 to 02:00 UTC to reflect the time they occurred in the WRF-Chem run. The ICEFLUX parameter is evaluated at 390 hPa.

increasing trend and variation in the LMA observations (Figure 12). This suggests the rapid intensification of the model storm may offset the delay in convective initiation.

6.2. Extended Evaluation

The WRF-Chem run was extended to 06:00 UTC model time (05:00 UTC observed time) for the six FRPSs discussed in Section 6.1 that provide the closest prediction of the number of flashes observed between 21:10 and 01:00 UTC observed time (Tables 3 and 4; Figure 13). This allowed for further comparison of the model-simulated flash rate time series during and after the primary peak in LMA observations. The observed and model-simulated flash rates are displayed in Figure 13 until 03:00 UTC observed time. After that time the observed flash rates become minimal.

Section 5.1 and Figures 4a–4f and 5a–5f compare the NEXRAD and WRF-Chem composite radar reflectivity until 02:30 UTC observed time (03:20 UTC model time) after which time the model simulation deviated from the observations. The extended WRF-Chem run shows that by 03:20 UTC model time (Figure 5f) the embedded convective cells are oriented in a similar west-east direction as the NEXRAD (02:30 UTC observed time; Figure 5e), although the WRF-Chem convective cells are intensifying on the northern edge of the system and the stratiform region is ∼60%–64% smaller than the observations. The simulated storm may have maintained its intensity for too long a period due to overestimation of hydrometeors that were not completely corrected by the damping and LDA techniques.

From 01:00 to 03:00 UTC observed time, the FRPSs based on UV and CTH are the only schemes in Figure 13 that simulate a peak at a similar time and magnitude as the LMA observations. However, the model-simulated flashes following the UV scheme decrease at a faster rate that is closer to that of the observed flashes. The UV scheme performed particularly well during the period of peak observed flash rates (00:40 to 02:00 UTC observed time). During this period the UV scheme has a mean bias of +17%. Over the shorter period from 01:30 to 02:00 UTC the bias was only +6%. The peak flash rate was overestimated by only 4.5%. During this same time period the flash

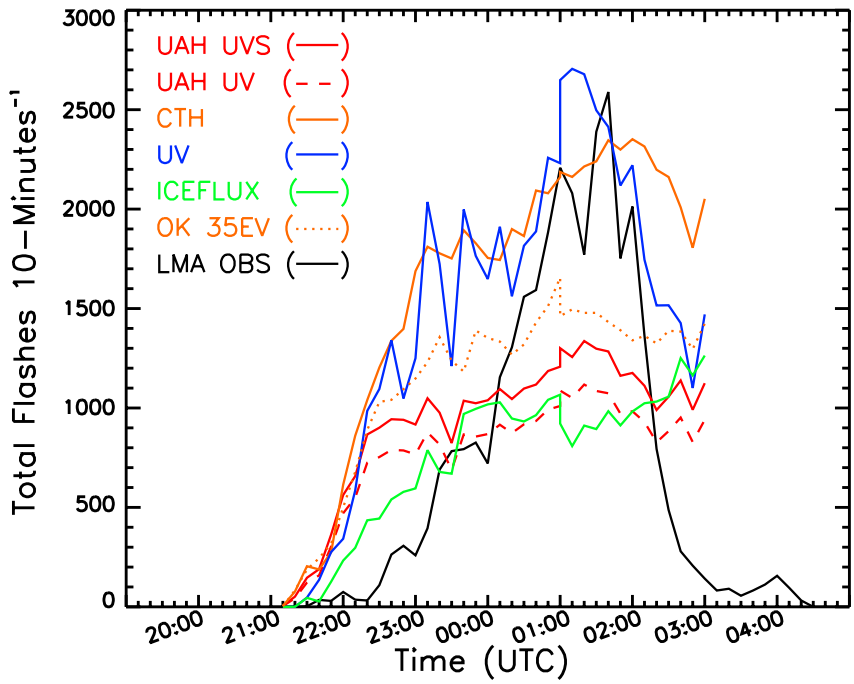

Figure 13. Same as Figure 8, except the FRPSs are based on relationships between storm parameters and total lightning activity with an overall total lightning flash count most similar to the Oklahoma LMA observations for the 21:10–01:00 UTC period. Also included are the extended WRF-Chem run predicted flashes from 02:00 to 04:00 UTC model time (01:00–03:00 UTC observed time). Each FRPS time series is adjusted 60 min earlier to coincide with the observed storm initiation time (21:10 UTC). The ICEFLUX parameter is evaluated at 390 hPa.

rate trends for three FRPSs (UAH UV, UAH UVS, OK 35EV) appear to slowly decrease, while for the ICEFLUX scheme the trend slowly increases. The maximum flash rate magnitude reached by these four schemes is about half the amount of the observed peak at 01:40 UTC.

From a LNO_x chemistry perspective, it is important to properly simulate the total number of flashes, in addition to their variation. The individual 10-min flash rates from the ICEFLUX scheme were only close to the observed rates from storm initiation until 00:00 UTC observed time. The total observed and simulated flash counts were similar over the period in which NO_x was sampled by the aircraft (ending at 01:00 UTC observed time) and over the entire duration of the convection. Therefore, the ICEFLUX scheme was used in WRF-Chem simulations of LNO_x for this storm that are reported in the companion paper (Pickering et al., 2024). However, the UV scheme best represented the lightning flash rate fluctuations of all the 18 schemes after 00:00 UTC model time, specifically the magnitude of the primary peak and subsequent decreasing trend.

7. Discussion

The initial and mature stages of the 29–30 May 2012 severe supercell system were reproduced fairly well by WRF-Chem regarding its area, height, and vertical motion, as well as the instability of the storm environment. The WRF-Chem simulated radar depiction deviated significantly from the observed radar after 03:00 UTC observed time. Therefore, we do not extend the comparison of predicted flash rates with observations beyond this time. The majority of the FRPSs overpredict the total flashes even after adjusting the model-simulated hydrometeors to bring them closer to the proxy observations. Here we explore why the FRPSs succeeded and failed in reproducing features in the observed flash rate trends, as well as how the results compare against the performance of FRPSs in other cloud-resolved simulations.

7.1. Ice-Phase Hydrometeors

Hydrometeors from observed radar data are determined by a very different method than those derived from model output. Thirteen of the 18 FRPSs involve relationships between total lightning activity and hydrometeors themselves or via radar reflectivity. Fuzzy logic algorithms were used to derive hydrometeor types from polarimetric radar for eight of these 13 (i.e., PIM, IMFP, CSU PIM and GEV, and four UAH GEV). The fuzzy logic algorithms developed by Dolan et al. (2013) and Vivekanandan et al. (1999) contain 10 and 14 hydrometeor categories, respectively, while the microphysics schemes available in WRF-Chem have about five available. Both bulk and bin microphysics parameterization scheme options are provided in WRF-Chem. The bulk schemes, in addition to many of the bin schemes, separate ice particles into predefined categories (e.g., cloud ice, snow, graupel, and hail) and the particle size distributions vary slightly between schemes. The disadvantage of having multiple ice categories is that this distinct separation is not natural. Instead there should be a gradual transition between the different ice types (Morrison & Grabowski, 2008; Morrison et al., 2015). Carey et al. (2019) also suggest that for proper application of radar-based FRPSs, further investigation into potential observational radar errors using a large variety of convective cases would be beneficial to ensure that kinematic and microphysical parameters are determined similarly in both radar systems and cloud-resolved models.

The differences between how observed and model hydrometeors are defined and determined could explain why the observed lightning is overestimated. For our case study we define dense precipitating ice as hail in the Morrison 2-moment microphysics scheme as this is more appropriate for continental deep convection. This means hail was used when a FRPS indicated the use of graupel. For the GEV schemes, CSU (Basarab et al., 2015) included both low- and high-density graupel categories, while UAH (Carey et al., 2015) calculations only used grid boxes where the graupel/small hail category dominated. The difference in the number of hydrometeor categories and how specific hydrometeors are applied highlights a potential issue when calculating hydrometeor-based storm parameters.

The IMFP in our study produced the greatest overprediction of the 18 FRPSs, as indicated by the large bias in total flashes and fluctuations (Table 4), but reproduced flash rate trends similar to the 29–30 May observations. This result resembles that of Barthe et al. (2010) where IMFP (a) recreated the trends of the observed total lightning flash rate time series, especially for a severe versus airmass thunderstorm, (b) could not reproduce the magnitude, and (c) produced one of the larger overestimates for an airmass thunderstorm, as well as during the early portion of the multicell stage of a severe storm. The severe storm simulated by Barthe et al. (2010) also produced like features in the flash rate time series predicted by PIM and overestimated their magnitudes, which is similar to the result for our severe system. The uncertainty with IMFP and PIM may be related to assumptions made within a microphysics scheme, which may generate errors when calculating ice mass (Barthe et al., 2010). IMFP and PIM are reasonable schemes because they are based on storm characteristics involved with cloud electrification; however, they appear to be very dependent on the proper prediction of variables within model-simulated storms.

FRPSs may instead benefit from total lightning activity and storm parameter relationships that avoid using specific ice hydrometeors (e.g., graupel). The transition between ice types is not gradual in microphysics schemes that offer multiple ice-phase categories, such as the Morrison 2-moment. This characteristic may not be appropriate when trying to generate lightning with a FRPS that involves specific ice categories. A solution may be to use a scheme based on a single ice-phase category, such as the predicted particle properties (P3) scheme (Morrison et al., 2015). This scheme predicts mass and number mixing ratios of rain and cloud water, as well as four ice mixing ratio variables (i.e., total ice mass, rime ice mass, rime volume, and total number). One of the advantages of the P3 scheme is its ability to allow for smooth transitions as ice particles grow. A final version of this scheme was not available to test at the time of this analysis.

7.2. Development and Application Environments for FRPSs

The three FRPSs (CSU PIM, 35EV, and GEV) developed using isolated Colorado thunderstorms (Basarab et al., 2015) overestimated the total number of LMA flashes in the 29–30 May simulated storms. The CSU 35EV scheme was considered the most robust of the three schemes because it performed well (Basarab et al., 2015) in other areas (i.e., Oklahoma, northern Alabama, and Washington, D.C.), but the 29–30 May Oklahoma storms had deep warm cloud depth (2.6 km, which is deeper than typical Colorado storms (Basarab et al., 2015; Fuchs et al., 2015)) and developed in an environment with high NCAPE (0.30 m s^{-2}) and high vertical wind shear (25 m s^{-1}). According to Basarab et al. (2015), this convective environment does not lend itself to a successful

application of the CSU 35EV scheme because the observed storm developed in an environment that did not maximize the performance of the FRPS. In addition, the cell-tracking algorithm used by CSU identified a cell as convective if the areas covered by two reflectivity thresholds (i.e., 35 and 45 dBZ) each exceeded a specified threshold (Basarab et al., 2015; Fuchs et al., 2015). In our cloud-resolved application of the CSU FRPSs, it was assumed the 35 dBZ criterion with no area threshold would be sufficient to differentiate between convective and stratiform regions in the model-simulated storms. However, it is possible the simulated storm region >35 dBZ included non-convective areas, especially since the model cells were not as individualized as the observations.

The four UAH GEV schemes that are based on northern Alabama thunderstorms (Carey et al., 2015) all overestimated the observed 29–30 May Oklahoma total flash rates. However, the UAH UV scheme, which is applied between −10 and −40°C where w > 5 m s^{-1}, only overestimated the observed flashes by 6.7%. This was the best performing non-hydrometeor scheme in terms of total predicted flashes. This suggests that using a FRPS based on the criteria relevant to cloud electrification (i.e., temperature and vertical velocity) may be most appropriate for predicting flash rates if the model has difficulty simulating the hydrometeors. When supercell-only versions of the schemes are used, the overprediction is roughly 30% larger than when the versions using all convection types are considered, even though the 29–30 May system consisted of supercells.

The three CSU schemes and the four UAH GEV schemes represent linear relationships with total lightning activity in their respective regions. However, the flash rates observed over the lifetime of our 29–30 May Oklahoma case study (max = 312 flashes min^{-1}; mean = 75.5 flashes min^{-1}) are higher than the flash rates observed in the northern Alabama (max = 102 flashes min^{-1}; mean = 12.5 flashes min^{-1}) and Colorado (max = 287.8 flashes min^{-1}; mean = 53.9 flashes min^{-1}) thunderstorm data sets, which were used to develop their respective FRPSs. This suggests the coefficients associated with these linear schemes may not be appropriate for the Oklahoma region or our 29–30 May event, and extrapolation to higher flash rates may not be suitable. For example, Basarab (2015) evaluated the same Alabama thunderstorm (18 May 2012) as Carey et al. (2014) using similar FRPSs (e.g., GEV). The schemes developed using Colorado storms had different coefficients than those based on Alabama convection and therefore did not predict the observed flash rates and trends as well. This single case study suggests that FRPSs may not be applicable for use on storms outside of the region used to develop the scheme.

The LTG3 scheme developed by McCaul et al. (2009, 2020) has only been implemented in models with horizontal resolutions of 2–4 km and their initial sensitivity studies indicate that users may need to recalibrate the LTG3 scheme parameters if the selected microphysics and PBL schemes differ from what is used in the McCaul et al. (2020) reference WRF configuration run. While the flash rates do not increase as quickly after convective initiation as some of the other FRPSs predict, the trend does become steeper after roughly 40 min and overestimates the observations by a factor of 3.8. It is possible that using the LTG3 scheme at a 1 km horizontal resolution with 89 vertical levels is too fine and is resolving additional storm features as the system matures. The production of stronger vertical velocities than would occur at 2–4 km resolution is one possibility, which would lead to an overestimation of flashes; however, the maximum updraft speed generated during the simulation is within 5% of the observations, although located at a slightly higher altitude. It is also possible our combination of the Morrison 2-moment microphysics and YSU PBL schemes requires a recalibration of the LTG3 scheme for application in our case study. McCaul et al. (2020) note that the Morrison scheme produces a larger lightning threat areal coverage, possibly due to greater anvil ice production, and the associated flash rate density threshold may need to be slightly increased when the Morrison scheme is used. Since our study increased the minimum graupel mixing ratio threshold to 0.5 g kg^{-1} in each of the FRPSs to better represent the charging region, the LTG3 recalibration would need to be looked at closer.

7.3. Non-Linear FRPSs

The majority of the FRPSs are built using data from individual storms. This includes CTH and w_{max}, which were designed to represent a storm with one maximum value; however, these non-linear FRPS equations are applied per model processor in WRF-Chem. While the non-linear schemes (i.e., CTH and w_{max}) are generally applied in the manner they were intended (i.e., storm height is similar to the width of the processor), CTH roughly doubles the LMA observations and w_{max} overpredicts by a factor of 4 larger than CTH. For our case study, each processor covering the model domain is roughly 18 km × 19 km in area, which is slightly smaller than the horizontal dimension of the 29-30 May observed and simulated supercells. The width of the processors is only ∼13%–19%

larger than the maximum model-simulated storm height (~16 km). Even if a storm were smaller than a processor, the cell would eventually span multiple tiles unless it remained stationary and near the processor's center. This means additional total lightning flashes are generated by the non-linear schemes when the cell spans more than one processor.

The w_{max} FRPS was built using two non-linear schemes (Price & Rind, 1992), where the slightly non-linear relation between w_{max} and CTH is incorporated into the fifth-power relationship between CTH and flash rate. While the non-linearity of w_{max} may not pose a problem when it is applied to a single area that envelops the convection of interest, errors may be exacerbated when the non-linear scheme is applied to a cell spanning multiple processors. Barthe et al. (2010) suggested w_{max} works better for severe than for weak thunderstorms; however, they point out that w_{max} is dependent on the simulation's horizontal resolution.

Barthe et al. (2010) simulated lightning flash rates for an isolated severe storm observed during STERAO-A and an airmass thunderstorm over northern Alabama using WRF output. The results suggested that when an adjustment factor was applied to the storm parameter, CTH performed better for the airmass thunderstorm, while w_{max} predicted the flash rate well for the severe storm. Initial results by Cummings et al. (2013) also suggested w_{max} and CTH were good predictors of the observed flash trend of deep tropical island convection at the cloud-resolved scale. Wong et al. (2013) discussed the need for a "calibration factor" due to the resolution dependency of the Price and Rind (1992, 1994) CTH scheme. Allen and Pickering (2002) did not favor the CTH scheme because the fifth-power in the FRPS equation causes the scheme to be very sensitive to any biases in the CTH of model-simulated continental convection. Giannaros et al. (2017) also suggest CTH is a poor proxy for the intensity of convection and lightning activity and that tuning is almost always necessary when implementing parameterizations similar to Price and Rind (1992). In a study by Giannaros et al. (2015), when a masking filter was used in conjunction with CTH and a convective parameterization in WRF, more realistic lightning predictions were possible for 10 different convective events observed in Greece. The masking filter was only applied to the CTH scheme when specific total ice content, w_{max}, and CAPE thresholds were met.

Further investigation of the sensitivity of the non-linear, and linear, schemes to the number of model processors and resolution would require additional model runs at coarser resolutions. Initial analysis with the instantaneous model output every 10 min indicates a negligible change in the flash counts generated by the linear FRPSs without a *y*-intercept as resolution is increased from 1 to 2 km and 4 km to reflect an increase in processor scale; however, the UV FRPS, which is a linear scheme with a negative *y*-intercept, indicates a factor of 5 and factor of 60 decrease in the simulated flash counts as the resolution is modified. Barthe et al. (2010) found the flash rates predicted by a FRPS (i.e., w_{max}, CTH, UV, IWP, PIM, and IMFP) were similar for a severe storm at model resolutions of 500 m, 1 km, and 2 km, and for an airmass thunderstorm at 1 and 3 km resolution.

7.4. Vertical Velocity

The three FRPSs that produced flash counts closest to the observations over the 21:10 to 03:00 UTC observed time period were the ICEFLUX scheme (Finney et al., 2014), UAH UV scheme, and UAH UVS scheme. These schemes are dependent on model vertical velocity. While the ICEFLUX scheme is more complex because it involves several frozen hydrometeors and their fall speeds, it only evaluates these criteria at a specific pressure level. This scheme is related to the IMFP because it focuses on the intensity of the flux of nonprecipitation ice particles, not just the mass. The ICEFLUX scheme does best reproducing the total number of lightning flashes for our 29–30 May case from 21:10 to 01:00 UTC observed time (Table 4). It also generates a similar trend as the observations for roughly the first 4 hr after convective initiation; however, the increase of the flash rate is steeper than the initial observations, which causes the more detailed shape of the observed peaks to not be well replicated. This scheme is also similar to the upward convective mass flux scheme, which Allen and Pickering (2002) determined was able to generate flash rates fairly well at most locations in a global model. However, the ICEFLUX scheme failed to show a decreasing trend in flash rate after 02:00 UTC observed time. Given its performance in our case study and its inclusion of both vertical motion and ice particles, which are equally important for cloud electrification, we suggest the ICEFLUX scheme has promise for future use through at least the beginning of the mature stage of a severe supercell system at cloud-resolved scales.

Unlike the other FRPSs, the UV schemes have a specific vertical velocity criterion applied within the mixed-phased region. Other schemes are more complex, since they require additional criteria within the mixed-phase region, such as reflectivity and/or hydrometeors (see Table 1). Using a vertical motion threshold may help the

model focus on the charged portion of the convective cloud, since updrafts play an important role in supplying water vapor for particle growth, ice particle collisions, and charge separation. In the model simulations prior to and with the current damping and LDA methods, all of the UV schemes were considered to be among the best performing schemes (Table 4); however, the UV scheme by Deierling and Petersen (2008) best represented the lightning flash rate fluctuations of all the 18 schemes during the later stages of our severe system (after 02:00 UTC observed time).

7.5. Future Simulations

As new FRPSs are developed or evolve, it is suggested the schemes be assessed using the same set of convective events and same model configuration for evaluation. These events should represent thunderstorms of varying type, severity, location, and flash rates. A complex set of cases will help validate a FRPS's performance by ensuring the scheme is working in the same manner as it was intended and by testing the limits of its application. A similar conclusion is made by Carey et al. (2019) where it's suggested that further investigation into potential observational radar errors involving a large set of convective cases would be beneficial to ensure that kinematic and microphysical parameters are determined similarly in both radar systems and cloud-resolved models which will allow for proper application of radar-based FRPSs. Similar intercomparison studies have been performed in the past using specific weather phenomena (e.g., 10 July 1996 STERAO-A storm) to investigate the performance of LNO_x parameterization schemes (Barth et al., 2007), FRPSs (Barthe et al., 2010), and microphysics schemes (Morrison et al., 2015). This evaluation process will allow for a better understanding of the performance of each FRPS, especially when the schemes are tested on a new convective event. The conclusion of such work may be that no one scheme will work best for all types of storms, all regions, and all phases of storm life cycle. Additional efforts could test whether machine learning could produce a parameterization that performs well for many storms. The 29–30 May DC3 storm would be a good candidate for testing an explicit lightning scheme such as found in the WRF-ELEC model (Fierro et al., 2013; Mansell et al., 2010) and although computationally expensive, could also be combined with representation of LNO_x production.

It would also be beneficial to test the FRPSs using new cloud physics model approaches, such as the P3 microphysics scheme (Morrison et al., 2015), to determine if the single ice-phase category improves total lightning flash prediction. It is also suggested that an in-depth sensitivity study be conducted, which explores the impact of the model resolution and the number of model processors on FRPSs, especially those schemes that are non-linear or linear with non-zero *y*-intercepts.

8. Conclusions

Lightning is dependent on updraft intensity and the hydrometeors in the mixed-phase region of a convective cloud. Therefore, it is necessary that the inputs to FRPSs accurately represent the kinematic and microphysical characteristics of a simulated storm. Eighteen FRPSs were evaluated based on their performance in a cloud-resolved simulation of the 29–30 May 2012 severe supercell system that was observed in Oklahoma by ground-based and airborne measurements during DC3; a significant limitation of this evaluation, however, is that it applied the FRPSs to only one cloud-resolved thunderstorm simulation. The observed storm location, dimensions, and vertical motion are represented reasonably well by the WRF-Chem model prior to and with the convective damping and LDA assumptions. However, the damping and LDA improve the microphysics by providing a better representation of the anvil area and slightly reducing the maximum altitude and value of the graupel mixing ratio. The model storm initiation is delayed 1-hr compared with observed radar; however, the simulated radar reflectivity and flash rates indicate this offset is not maintained and ranges from 30 to 50 min as the storm evolves. To further improve the model-simulated hydrometeors' mixing ratio and vertical extent, altitude-specific scaling factors derived by comparison of the model output with DLA proxy observations are applied during the simulation to the hydrometeors in the FRPS code (i.e., the hydrometeors were not adjusted in the microphysics scheme), thereby adjusting the hydrometeors closer to the observations. The changes in model flash rates due to these adjustments highlight the dependency FRPSs have on the proper representation of storm parameters in models. The simulated storm maintained intensity for too long a period into the observed dissipation stage of the storm system. Therefore, the flash rate evaluation was terminated 2 hr prior to the end of the simulation.

The damping, LDA, and scaling of hydrometeors to proxy observations provided the best hydrometeor distribution and allowed for the comparison of observed and model-simulated total lightning flashes. The analysis showed that the LMA observations were well represented by two schemes. The ICEFLUX scheme (Finney et al., 2014) most closely replicated the observed flash rate trends during the first 4 hr of convection, which is important for the LNO_x simulation reported in the companion paper (Pickering et al., 2024). ICEFLUX also provided the best estimate of the total flashes over the entire simulation. However, this scheme is very sensitive to the pressure level at which it is evaluated and may require adjustment when simulating other convective events at cloud-resolved scales. The LNO_x simulation in the companion paper results in a rather low value of mean LNO_x production per flash, in agreement with the findings of Pollack et al. (2016) that are based solely on aircraft observations, yielding important validation of both their methodology and the model-based approach. The UV scheme (Deierling & Petersen, 2008) provided predicted flashes that compared well with observations during the later lifecycle stages of the severe supercell system. The UV scheme best represents the observed flashes during the period of the peak flash rate (00:40–02:20 UTC observed time) and the subsequent period of sharp flash rate decline. The three FRPSs that produced the total flash counts closest to the observational total over the entire evaluation period were the ICEFLUX, UAH UV, and UAH UVS schemes, indicating that the latter two of these schemes may be additional candidate schemes for use in chemistry simulations.

Data Availability Statement

Observational Data Availability: A majority of the DC3 field campaign data used in this work are provided by NCAR/Earth Observing Laboratory under the sponsorship of the National Science Foundation (NCAR, 2012a), including the GOES-13 visible satellite imagery data (NCAR, 2012b), the NSSL MGAUS Oklahoma-Texas sounding data (Ziegler, 2013a), and the Oklahoma LMA data (Bruning, 2014). NLDN data are available for purchase from Vaisala, Inc. ENTLN data are available upon request from Earth Networks, Inc.

Model Data Availability: The original source code for the WRF-Chem model version 3.6.1 (NCAR, 2014) is modified for our FRPS simulations and is available at https://dsrs.atmos.umd.edu/DATA/WRF-ChemV3.6.1-modified-scripts/ (FRPS, 2023a). In addition to the NAM-ANL model forecast data (NOAA, 2012), specific files that may be useful in rerunning the WRF-Chem simulation are available at https://dsrs.atmos.umd.edu/DATA/run-WRF-ChemV3.6.1-files/ (FRPS, 2023b). A sub-set of the model output and a restart file are available at https://dsrs.atmos.umd.edu/DATA/FRPS/ (FRPS, 2023c).

Acknowledgments
K. A. Cummings would like to thank the National Science Foundation (NSF) for funding a portion of this work under Grants NSF-1063479 and AGS-1522551. Cummings was employed by NASA through the NASA Pathways Program during completion of this research; however, the article was written on behalf of the University of Maryland. K. E. Pickering was supported by the NASA Aura Validation Program and the NASA Atmospheric Composition Data Analysis and Modeling (ACCDAM) Program. Y. Li and D. Allen were supported by the aforementioned NSF grants. NCAR is sponsored by the NSF. M. C. Barth was supported by NSF Grant 0856145. M. M. Bela was supported by NASA ACCDAM Grant NNX14AR56G, a National Research Council Research Associateship Programs Postdoctoral Fellowship, and by the NOAA Cooperative Agreement with CIRES, NA17OAR4320101. E. Bruning was supported by Grant NSF-1063966. D. R. MacGorman and C. Ziegler were supported by NSF Grant AGS-1063945. M. I. Biggerstaff was supported by NSF Grant AGS-1063537. B. Fuchs and T. Davis were supported by NSF PDM Grant AGS-1429925. L. Carey and R. Mecikalski were supported by NSF PDM Grant AGS-1063573. D. L. Finney was supported by a Natural Environment Research Council Grant NE/K500835/1. We gratefully acknowledge V. Chmielewski (Texas Tech University) for discussing the detection efficiencies of the central Oklahoma LMA network; S. Rutledge (CSU) for his helpful discussions in the development of a FRPS for the Oklahoma observed severe supercell system; B. Basarab (Global Weather Corporation, formerly CSU) for his assistance in interpreting the CSU-developed FRPSs for application in the model; and T. Mansell (NOAA/NSSL), E. DiGangi, and D. Betten (University of Oklahoma) for their involvement in generating and discussing the DLA model output. A special thanks is offered to H. Morrison (NCAR) for his helpful feedback and suggestions for investigating the microphysics results, and E. McCaul (Universities Space Research Association) for his discussions and assistance in implementing the lightning threat method. We also thank NCAR/Computational Information Systems Laboratory for use of the Yellowstone and Cheyenne supercomputers and C. Homeyer (University of Oklahoma) for providing regional NEXRAD level II data.

References

Adams-Selin, R. D., van den Heever, S. C., & Johnson, R. H. (2013). Impact of graupel parameterization schemes on idealized bow echo simulations. *Monthly Weather Review*, *141*(4), 1241–1262. https://doi.org/10.1175/MWR-D-12-00064.1

Allen, D. J., & Pickering, K. E. (2002). Evaluation of lightning flash rate parameterizations for use in a global chemical transport model. *Journal of Geophysical Research*, *107*(D23), 4711. https://doi.org/10.1029/2002JD002066

Barth, M. C., Cantrell, C. A., Brune, W. H., Rutledge, S. A., Crawford, J. H., Huntrieser, H., et al. (2015). The deep convective clouds and chemistry (DC3) field campaign. *Bulletin of the American Meteorology Society*, *96*(8), 1281–1309. https://doi.org/10.1175/BAMS-D-13-00290.1

Barth, M. C., Kim, S.-W., Skamarock, W. A., Stuart, A. L., Pickering, K. E., & Ott, L. E. (2007). Simulations of the redistribution of formaldehyde, formic acid, and peroxides in the 10 July 1996 Stratospheric-Tropospheric Experiment: Radiation, Aerosols, and Ozone deep convection storm. *Journal of Geophysical Research*, *112*(D13), D13310. https://doi.org/10.1029/2006JD008046

Barthe, C., & Barth, M. C. (2008). Evaluation of a new lightning-produced NO_x parameterization for cloud resolving models and its associated uncertainties. *Atmospheric Chemistry and Physics*, *8*(16), 4691–4710. https://doi.org/10.5194/acp-8-4691-2008

Barthe, C., Deierling, W., & Barth, M. C. (2010). Estimation of total lightning from various storm parameters: A cloud-resolving model study. *Journal of Geophysical Research*, *115*(D24), D24202. https://doi.org/10.1029/2010JD014405

Barthe, C., Molinié, G., & Pinty, J.-P. (2005). Description and first results of an explicit electrical scheme in a 3D cloud resolving model. *Atmospheric Research*, *76*(1–4), 95–113. https://doi.org/10.1016/j.atmosres.2004.11.021

Basarab, B. M. (2015). Prediction of total lightning in Colorado and Alabama thunderstorms based on storm dynamical and microphysical variables. (M.S. thesis). Colorado State University. Retrieved from http://hdl.handle.net/10217/166859

Basarab, B. M., Rutledge, S. A., & Fuchs, B. R. (2015). An improved lightning flash rate parameterization developed from Colorado DC3 thunderstorm data for use in cloud-resolving chemical transport models. *Journal of Geophysical Research: Atmospheres*, *120*(18), 9481–9499. https://doi.org/10.1002/2015JD023470

Bela, M. M., Barth, M. C., Toon, O. B., Fried, A., Homeyer, C. R., Morrison, H., et al. (2016). Wet scavenging of soluble gases in DC3 deep convective storms using WRF-Chem simulations and aircraft observations. *Journal of Geophysical Research: Atmospheres*, *121*(8), 4233–4257. https://doi.org/10.1002/2015JD024623

Benjamin, S. G., Weygandt, S. S., Brown, J. M., Hu, M., Alexander, C. R., Smirnova, T. G., et al. (2016). A North American hourly assimilation and model forecast cycle: The rapid refresh. *Monthly Weather Review*, *144*(4), 1669–1694. https://doi.org/10.1175/MWR-D-15-0242.1

Bovalo, C., Barthe, C., & Pinty, J.-P. (2019). Examining relationships between cloud-resolving model parameters and total flash rates to generate lightning density maps. *Quarterly Journal of the Royal Meteorological Society*, *145*(720), 1250–1266. https://doi.org/10.1002/qj.3494

Bruning, E. (2014). DC3: OKLMA HDF5 flash data and NetCDF grids. Version 1.0 [Dataset]. *UCAR/NCAR—Earth Observing Laboratory*. https://doi.org/10.26023/J9JZ-S43M-DY13

Bryan, G. H., & Morrison, H. (2012). Sensitivity of a simulated squall line to horizontal resolution and parameterization of microphysics. *Monthly Weather Review*, *140*(1), 202–225. https://doi.org/10.1175/MWR-D-11-00046.1

Carey, L. D., Bain, A. L., & Matthee, R. (2014). *Kinematic and microphysical control of lightning in multicell convection over Alabama during DC3*. Paper presented at 23rd international lightning detection conference/5th international lightning meteorology conference. Vaisala, Inc.

Carey, L. D., & Rutledge, S. A. (1996). A multiparameter radar case study of the microphysical and kinematic evolution of a lightning producing storm. *Meteorology and Atmospheric Physics*, *59*(1–2), 33–64. https://doi.org/10.1007/BF01032000

Carey, L. D., Schultz, E. V., Schultz, C. J., Bain, A. L., Mecikalski, R. M., Deierling, W., et al. (2015). *Kinematic and microphysical control of lightning flash rate over northern Alabama*. Paper presented at 7th conference on the meteorological applications of lightning data. American Meteorological Society.

Carey, L. D., Schultz, E. V., Schultz, C. J., Deierling, W., Petersen, W. A., Bain, A. L., & Pickering, K. E. (2019). An evaluation of relationships between radar-inferred kinematic and microphysical parameters and lightning flash rates in Alabama storms. *Atmosphere*, *10*(12), 796. https://doi.org/10.3390/atmos10120796

Chmielewski, V. C., & Bruning, E. C. (2016). Lightning mapping array flash detection performance with variable receiver thresholds. *Journal of Geophysical Research: Atmospheres*, *121*(14), 8600–8614. https://doi.org/10.1002/2016JD025159

Chmielewski, V. C., MacGorman, D. R., Ziegler, C. L., DiGangi, E., Betten, D., & Biggerstaff, M. (2020). Microphysical and transportive contributions to normal and anomalous polarity subregions in the 29-30 May 2012 Kingfisher storm. *Journal of Geophysical Research: Atmospheres*, *125*(16), e2020JD032384. https://doi.org/10.1029/2020JD032384

Christian, H. J., Blakeslee, R. J., Boccippio, D. J., Boeck, W. L., Buechler, D. E., Driscoll, K. T., et al. (2003). Global frequency and distribution of lightning as observed from space by the Optical Transient Detector. *Journal of Geophysical Research*, *108*(D1), 4005. https://doi.org/10.1029/2002JD002347

Cummings, K. A., Huntemann, T. L., Pickering, K. E., Barth, M. C., Skamarock, W. C., Höller, H., et al. (2013). Cloud-resolving chemistry simulation of a Hector thunderstorm. *Atmospheric Chemistry and Physics*, *13*(5), 2757–2777. https://doi.org/10.5194/acp-13-2757-2013

Cummins, K. L., & Murphy, M. J. (2009). An overview of lightning locating systems: History, techniques, and data uses, with an in-depth look at the U.S. NLDN. *IEEE Transactions on Electromagnetic Compatibility*, *51*(3), 499–518. https://doi.org/10.1109/TEMC.2009.2023450

Davenport, C. E., Ziegler, C. L., & Biggerstaff, M. I. (2019). Creating a more realistic idealized supercell thunderstorm evolution via incorporation of base-state environmental variability. *Monthly Weather Review*, *147*(11), 4177–4198. https://doi.org/10.1175/MWR-D-18-0447.1

Deierling, W. (2006). The relationship between total lightning and ice fluxes. (Doctoral dissertation). University of Alabama in Huntsville.

Deierling, W., & Petersen, W. A. (2008). Total lightning activity as an indicator of updraft characteristics. *Journal of Geophysical Research*, *113*(D16), D16210. https://doi.org/10.1029/2007JD009598

Deierling, W., Petersen, W. A., Latham, J., Ellis, S., & Christian, H. J. (2008). The relationship between lightning activity and ice fluxes in thunderstorms. *Journal of Geophysical Research*, *113*(D15), D15210. https://doi.org/10.1029/2007JD009700

DiGangi, E. (2014). *A study of the electrical, microphysical, and kinematic properties of the 29 May Kingfisher supercell*. (M.S. thesis). University of Oklahoma. Retrieved from http://hdl.handle.net/11244/14246

DiGangi, E. A., MacGorman, D. R., Ziegler, C. L., Betten, D., Biggerstaff, M., Bowlan, M., & Potvin, C. (2016). An overview of the 29 May 2012 Kingfisher supercell during DC3. *Journal of Geophysical Research: Atmospheres*, *121*(24), 14316–14343. https://doi.org/10.1002/2016JD025690

DiGangi, E. A., Ziegler, C. L., & MacGorman, D. R. (2021). Lightning and secondary convection in the anvil of the May 29, 2012 Oklahoma supercell storm observed by DC3. *Journal of Geophysical Research: Atmospheres*, *126*(3), e2020JD033114. https://doi.org/10.1029/2020JD033114

Dolan, B., Rutledge, S. A., Lim, S., Chandrasekar, V., & Thurai, M. (2013). A robust C-band hydrometeor identification algorithm and application to a long-term polarimetric radar dataset. *Journal of Applied Meteorology and Climatology*, *52*(9), 2162–2186. https://doi.org/10.1175/JAMC-D-12-0275.1

Fierro, A. O., Clark, A. J., Mansell, E. R., MacGorman, D. R., Dembek, S. R., & Ziegler, C. L. (2015). Impact of storm-scale lightning data assimilation on WRF-ARW precipitation forecasts during the 2013 warm season over the contiguous United States. *Monthly Weather Review*, *143*(3), 757–777. https://doi.org/10.1175/MWR-D-14-00183.1

Fierro, A. O., Gao, J., Ziegler, C. L., Calhoun, K. M., Mansell, E. R., & MacGorman, D. R. (2016). Assimilation of flash extent data in the variational framework at convection-allowing scales: Proof-of-concept and evaluation for the short-term forecast of the 24 May 2011 tornado outbreak. *Monthly Weather Review*, *144*(11), 4373–4393. https://doi.org/10.1175/MWR-D-16-0053.1

Fierro, A. O., Gao, J., Ziegler, C. L., Mansell, E. R., MacGorman, D. R., & Dembek, S. R. (2014). Evaluation of a cloud-scale lightning data assimilation technique and a 3DVAR method for the analysis and short-term forecast of the 29 June 2012 derecho event. *Monthly Weather Review*, *142*(1), 183–202. https://doi.org/10.1175/MWR-D-13-00142.1

Fierro, A. O., Mansell, E. R., MacGorman, D. R., & Ziegler, C. L. (2013). The implementation of an explicit charging and discharge lightning scheme within the WRF-ARW model: Benchmark simulations of a continental squall line, a tropical cyclone, and a winter storm. *Monthly Weather Review*, *141*(7), 2390–2415. https://doi.org/10.1175/MWR-D-12-00278.1

Fierro, A. O., Mansell, E. R., Ziegler, C. L., & MacGorman, D. R. (2012). Application of a lightning data assimilation technique in the WRF-ARW model at cloud-resolving scales for the tornado outbreak of 24 May 2011. *Monthly Weather Review*, *140*(8), 2609–2627. https://doi.org/10.1175/MWR-D-11-00299.1

Finney, D. L., Doherty, R. M., Wild, O., Huntrieser, H., Pumphrey, H. C., & Blyth, A. M. (2014). Using cloud ice flux to parametrise large-scale lightning. *Atmospheric Chemistry and Physics*, *14*(23), 12665–12682. https://doi.org/10.5194/acp-14-12665-2014

FRPS. (2023a). Modified WRF-ChemV3.6.1 scripts [Software]. Retrieved from https://dsrs.atmos.umd.edu/DATA/WRF-ChemV3.6.1-modified-scripts/

FRPS. (2023b). WRF-ChemV3.6.1 data input files [Dataset]. Retrieved from https://dsrs.atmos.umd.edu/DATA/run-WRF-ChemV3.6.1-files/

FRPS. (2023c). WRF-ChemV3.6.1 model output and restart files [Dataset]. Retrieved from https://dsrs.atmos.umd.edu/DATA/FRPS/

Fuchs, B. R., Rutledge, S. A., Bruning, E. C., Pierce, J. R., Kodros, J. K., Lang, T. J., et al. (2015). Environmental controls on storm intensity and charge structure in multiple regions of the continental United States. *Journal of Geophysical Research: Atmospheres*, *120*(13), 6575–6596. https://doi.org/10.1002/2015JD023271

Giannaros, T., Kotroni, V., & Lagouvardos, K. (2015). Predicting lightning activity in Greece with the Weather Research and Forecasting (WRF) model. *Atmospheric Research*, *156*, 1–13. https://doi.org/10.1016/j.atmosres.2014.12.009

Giannaros, T. M., Lagouvardos, K., & Kotroni, V. (2017). Performance evaluation of an operational lightning forecasting system in Europe. *Natural Hazards*, *85*, 1–18. https://doi.org/10.1007/s11069-016-2555-y

Heckman, S., & Liu, C. (2010). *The application of total lightning detection for severe storm prediction*. Paper presented at 10th European conference on applications of meteorology. European Meteorological Society.

Helsdon, J. H., Jr., Wu, G., & Farley, R. D. (1992). An intracloud lightning parameterization scheme for a storm electrification model. *Journal of Geophysical Research*, *97*(D5), 5865–5884. https://doi.org/10.1029/92JD00077

Heymsfield, A. J., & Miller, K. M. (1988). Water vapor and ice mass transported into the anvils of CCOPE thunderstorms: Comparison with storm influx and rainout. *Journal of the Atmospheric Sciences*, *45*(22), 3501–3514. https://doi.org/10.1175/1520-0469(1988)045<3501:WVAIMT>2.0.CO;2

Heymsfield, A. J., & Palmer, A. G. (1986). Relationships for deriving thunderstorm anvil ice mass for CCOPE storm water budget estimates. *Journal of Applied Meteorology and Climatology*, *25*(5), 691–702. https://doi.org/10.1175/1520-0450(1986)025<0691:RFDTAI>2.0.CO;2

Holle, R. L., Demetriades, N. W. S., & Nag, A. (2014). *Lightning warnings with NLDN cloud and cloud-to-ground lightning data*. Paper presented at 23rd international lightning detection conference/5th international lightning meteorology conference. Vaisala, Inc.

Jayaratne, E. R., Saunders, C. P. R., & Hallett, J. (1983). Laboratory studies of the charging of soft-hail during ice crystal interactions. *Quarterly Journal of the Royal Meteorological Society*, *109*(461), 609–630. https://doi.org/10.1002/qj.49710946111

Krehbiel, P. R., Thomas, R. J., Rison, W., Hamlin, T., Harlin, J., & Davis, M. (2000). GPS-based mapping system reveals lightning inside storms. *Eos, Transactions American Geophysical Union*, *81*(3), 21–25. https://doi.org/10.1029/00EO00014

Latham, J., Petersen, W. A., Deierling, W., & Christian, H. J. (2007). Field identification of a unique globally dominant mechanism of thunderstorm electrification. *Quarterly Journal of the Royal Meteorological Society*, *133*(627), 1453–1457. https://doi.org/10.1002/qj.133

Li, Y., Pickering, K. E., Allen, D. J., Barth, M. C., Bela, M. M., Cummings, K. A., et al. (2017). Evaluation of deep convective transport in storms from different convective regimes during the DC3 field campaign using WRF-Chem with lightning data assimilation. *Journal of Geophysical Research: Atmospheres*, *122*(13), 7140–7163. https://doi.org/10.1002/2017JD026461

Liu, C., Cecil, D. J., Zipser, E. J., Kronfeld, K., & Robertson, R. (2012). Relationships between lightning flash rates and radar reflectivity vertical structures in thunderstorms over the tropics and subtropics. *Journal of Geophysical Research*, *117*(D6), D06212. https://doi.org/10.1029/2011JD017123

Liu, C., & Heckman, S. (2011). *The application of total lightning detection and cell tracking for severe weather prediction*. Paper presented at 5th conference on the meteorological applications of lightning data. American Meteorological Society.

Lopez, P. (2016). A lightning parameterization for the ECMWF integrated forecasting system. *Monthly Weather Review*, *144*(9), 3057–3075. https://doi.org/10.1175/MWR-D-16-0026.1

Lund, N. R., MacGorman, D. R., Schuur, T. J., Biggerstaff, M. I., & Rust, W. D. (2009). Relationships between lightning location and polarimetric radar signatures in a small mesoscale convective system. *Monthly Weather Review*, *137*(12), 4151–4170. https://doi.org/10.1175/2009MWR2860.1

Lynn, B. H., Yair, Y., Price, C., Kelman, G., & Clark, A. (2012). Predicting cloud-to-ground and intracloud lightning in weather forecast models. *Weather and Forecasting*, *27*(6), 1470–1488. https://doi.org/10.1175/WAF-D-11-00144.1

MacGorman, D. R., & Rust, W. D. (1998). *The electrical nature of storms*. Oxford University Press.

MacGorman, D. R., Straka, J. M., & Ziegler, C. L. (2001). A lightning parameterization for numerical cloud models. *Journal of Applied Meteorology and Climatology*, *40*(3), 459–478. https://doi.org/10.1175/1520-0450(2001)040<0459:ALPFNC>2.0.CO;2

Mansell, E. R., MacGorman, D. R., Ziegler, C. L., & Straka, J. M. (2002). Simulated three-dimensional branched lightning in a numerical thunderstorm model. *Journal of Geophysical Research*, *107*(D9), ACL2-1–ACL2-12. https://doi.org/10.1029/2000JD000244

Mansell, E. R., Ziegler, C. L., & Bruning, E. C. (2010). Simulated electrification of a small thunderstorm with two-moment bulk microphysics. *Journal of the Atmospheric Sciences*, *67*(1), 171–194. https://doi.org/10.1175/2009JAS2965.1

Marchand, M. R., & Fuelberg, H. E. (2014). Assimilation of lightning data using a nudging method involving low-level warming. *Monthly Weather Review*, *142*(12), 4850–4871. https://doi.org/10.1175/MWR-D-14-00076.1

McCaul, E. W., Goodman, S. J., LaCasse, K. M., & Cecil, D. J. (2009). Forecasting lightning threat using cloud-resolved model simulations. *Weather and Forecasting*, *24*(3), 709–729. https://doi.org/10.1175/2008WAF2222152.1

McCaul, E. W., Jr., Priftis, G., Case, J. L., Chronis, T., Gatlin, P. N., Goodman, S. J., & Kong, F. (2020). Sensitivities of the WRF lightning forecast algorithm to parameterized microphysics and boundary layer schemes. *Weather and Forecasting*, *35*(4), 1545–1560. https://doi.org/10.1175/WAF-D-19-0101.1

Mecikalski, R. M., & Carey, L. D. (2017). Lightning characteristics relative to radar, altitude and temperature for a multicell, MCS and supercell over northern Alabama. *Atmospheric Research*, *191*, 128–140. https://doi.org/10.1016/j.atmosres.2017.03.001

Morrison, H., & Grabowski, W. W. (2008). A novel approach for representing ice microphysics in models: Description and tests using a kinematic framework. *Journal of the Atmospheric Sciences*, *65*(5), 1528–1548. https://doi.org/10.1175/2007JAS2491.1

Morrison, H., & Milbrandt, J. A. (2011). Comparison of two-moment bulk microphysics schemes in idealized supercell thunderstorm simulations. *Monthly Weather Review*, *139*(4), 1103–1130. https://doi.org/10.1175/2010MWR3433.1

Morrison, H., Milbrandt, J. A., Bryan, G. H., Ikeda, K., Tessendorf, S. A., & Thompson, G. (2015). Parameterization of cloud microphysics based on the prediction of bulk ice particle properties. Part II: Case study comparisons with observations and other schemes. *Journal of the Atmospheric Sciences*, *72*(1), 312–339. https://doi.org/10.1175/JAS-D-14-0066.1

Nag, A., Mallick, S., Rakov, V. A., Howard, J. S., Biagi, C. J., Hill, J. D., et al. (2011). Evaluation of U.S. National Lightning Detection Network performance characteristics using rocket-triggered lightning data acquired in 2004-2009. *Journal of Geophysical Research*, *116*(D2), D02123. https://doi.org/10.1029/2010JD014929

NCAR. (2012a). DC3: Deep convective clouds & chemistry project [Dataset]. *UCAR/NCAR—Earth Observing Laboratory*. Retrieved from https://data.eol.ucar.edu/project/353

NCAR. (2012b). GOES-13 visible satellite images [Dataset]. *UCAR/NCAR—Earth Observing Laboratory*. Retrieved from http://catalog.eol.ucar.edu/cgi-bin/dc3_2012/ops/index

NCAR. (2014). WRF-Chem model version 3.6.1 [Software]. Retrieved from https://www2.mmm.ucar.edu/wrf/users/download/get_source.html

NOAA. (2012). NAM-ANL forecast model data [Dataset]. Retrieved from https://www.ncei.noaa.gov/products/weather-climate-models/north-american-mesoscale

Orville, R. E., & Henderson, R. W. (1986). Global distribution of midnight lightning: September 1977 to August 1978. *Monthly Weather Review*, *114*(12), 2640–2653. https://doi.org/10.1175/1520-0493(1986)114<2640:GDOMLS>2.0.CO;2

Petersen, W. A., Christian, H. J., & Rutledge, S. A. (2005). TRMM observations of the global relationship between ice water content and lightning. *Geophysical Research Letters*, *32*(14), L14819. https://doi.org/10.1029/2005GL023236

Pickering, K. E., Li, Y., Cummings, K. A., Barth, M. C., Allen, D. J., Bruning, E., & Pollack, I. (2024). Lightning NO_x in the May 29-30, 2012 deep convective clouds and chemistry (DC3) severe storm and its downwind chemical consequences. *Journal of Geophysical Research: Atmospheres*, *124*(13), 7413–7428. https://doi.org/10.1029/2023JD039439

Pickering, K. E., Wang, Y., Tao, W.-K., Price, C., & Müller, J.-F. (1998). Vertical distributions of lightning NOx for use in regional and global chemical transport models. *Journal of Geophysical Research*, *103*(D23), 31203–31216. https://doi.org/10.1029/98JD02651

Pollack, I. B., Homeyer, C. R., Ryerson, T. B., Aikin, K. C., Peischl, J., Apel, E. C., et al. (2016). Airborne quantification of upper tropospheric NOx production from lightning in deep convective storms over the United States Great Plains. *Journal of Geophysical Research: Atmospheres*, *121*(4), 2002–2028. https://doi.org/10.1002/2015JD023941

Price, C., & Rind, D. (1992). A simple lightning parameterization for calculating global lightning distributions. *Journal of Geophysical Research*, *97*(D9), 9919–9933. https://doi.org/10.1029/92JD00719

Price, C., & Rind, D. (1994). Modeling global lightning distributions in a general circulation model. *Monthly Weather Review*, *122*(8), 1930–1939. https://doi.org/10.1175/1520-0493(1994)122<1930:MGLDIA>2.0.CO;2

Qian, X., & Wang, H. (2021). Evaluation of different storm parameters as the proxies for gridded total lightning flash rates: A convection-allowing model study. *Atmosphere*, *12*(1), 95. https://doi.org/10.3390/atmos12010095

Rakov, V. A. (2016). Electrical structure of thunderclouds. In *Fundamentals of lightning* (pp. 31–51). Cambridge University Press.

Rison, W., Thomas, R. J., Krehbiel, P. R., Hamlin, T., & Harlin, J. (1999). A GPS-based three-dimensional lightning mapping system: Initial observations in central New Mexico. *Geophysical Research Letters*, *26*(23), 3573–3576. https://doi.org/10.1029/1999GL010856

Romps, D. M. (2019). Evaluating the future of lightning in cloud-resolving models. *Geophysical Research Letters*, *46*(24), 14863–14871. https://doi.org/10.1029/2019GL085748

Rossow, W. B., Walker, A. W., Beuschel, D. E., & Roiter, M. D. (1996). *International Satellite Cloud Climatology Project (ISCCP) documentation of new cloud data sets. WMO/TD 737*. World Meteorological Organization.

Saunders, C. P. R., Keith, W. D., & Mitzeva, R. P. (1991). The effect of liquid water on thunderstorm charging. *Journal of Geophysical Research*, *96*(D6), 11007–11017. https://doi.org/10.1029/91JD00970

Schwartz, C. S., Romine, G. S., Sobash, R. A., Fossell, K. R., & Weisman, M. L. (2015). NCAR's experimental real-time convection-allowing ensemble prediction system. *Weather and Forecasting*, *30*(6), 1645–1654. https://doi.org/10.1175/WAF-D-15-0103.1

Takahashi, T. (1978). Riming electrification as a charge generation mechanism in thunderstorms. *Journal of the Atmospheric Sciences*, *35*(8), 1536–1548. https://doi.org/10.1175/1520-0469(1978)035<1536:REAACG>2.0.CO;2

Thomas, R. J., Krehbiel, P. R., Rison, W., Hunyady, S. J., Winn, W. P., Hamlin, T., & Harlin, J. (2004). Accuracy of the lightning mapping array. *Journal of Geophysical Research*, *109*(D14), D14207. https://doi.org/10.1029/2004JD004549

Turman, B. N. (1978). Analysis of lightning data from the DMSP satellite. *Journal of Geophysical Research*, *83*(C10), 5019–5024. https://doi.org/10.1029/JC083iC10p05019

Van Weverberg, K. (2013). Impact of environmental instability on convective precipitation uncertainty associated with the nature of the rimed ice species in a bulk microphysics scheme. *Monthly Weather Review*, *141*(8), 2841–2849. https://doi.org/10.1175/MWR-D-13-00036.1

Vivekanandan, J., Zrnic, D. S., Ellis, S., Oye, R., Ryzhkov, A. V., & Straka, J. (1999). Cloud microphysics retrievals using S-band dual-polarization radar measurements. *Bulletin of the American Meteorological Society*, *80*(3), 381–388. https://doi.org/10.1175/1520-0477(1999)080<0381:CMRUSB>2.0.CO;2

Waugh, S. M., Ziegler, C. L., & MacGorman, D. R. (2018). In situ microphysical observations of the 29-30 May 2012 Kingfisher, OK supercell with a balloon-borne video disdrometer. *Journal of Geophysical Research: Atmospheres*, *123*(10), 5618–5640. https://doi.org/10.1029/2017JD027623

Wiens, K. C., Rutledge, S. A., & Tessendorf, S. A. (2005). The 29 June 2000 supercell observed during STEPS. Part II: Lightning and charge structure. *Journal of the Atmospheric Sciences*, *62*(12), 4151–4177. https://doi.org/10.1175/JAS3615.1

Wilkinson, J. M., & Bornemann, F. J. (2014). A lightning forecast for the London 2012 Olympics opening ceremony. *Weather*, *69*(1), 16–19. https://doi.org/10.1002/wea.2176

Williams, E. R. (1985). Large-scale charge separation in thunderclouds. *Journal of Geophysical Research*, *90*(D4), 6013–6025. https://doi.org/10.1029/JD090iD04p06013

Wong, J., Barth, M. C., & Noone, D. (2013). Evaluating a lightning parameterization based on cloud-top height for mesoscale numerical simulations. *Geoscientific Model Development*, *6*(2), 429–443. https://doi.org/10.5194/gmd-6-429-2013

Yair, Y., Lynn, B. H., Price, C., Kotroni, V., Lagouvardos, K., Morin, E., et al. (2010). Predicting the potential for lightning activity in Mediterranean storms based on the Weather Research and Forecasting (WRF) model dynamic and microphysical fields. *Journal of Geophysical Research*, *115*(D4), D04205. https://doi.org/10.1029/2008JD010868

Ziegler, C. (2013a). NSSL MGAUS Oklahoma-Texas sounding data. Version 1.0 [Dataset]. *UCAR/NCAR—Earth Observing Laboratory*. https://doi.org/10.5065/D63R0R84

Ziegler, C. L. (2013b). A diabatic Lagrangian technique for the analysis of convective storms. Part I: Description and validation via an observing system simulation experiment. *Journal of Atmospheric and Oceanic Technology*, *30*(10), 2248–2265. https://doi.org/10.1175/JTECH-D-12-00194.1

Ziegler, C. L. (2013c). A diabatic Lagrangian technique for the analysis of convective storms. Part II: Application to a radar-observed storm. *Journal of Atmospheric and Oceanic Technology*, *30*(10), 2266–2280. https://doi.org/10.1175/JTECH-D-13-00036.1

Zipser, E. J., & Lutz, K. R. (1994). The vertical profile of radar reflectivity of convective cells: A strong indicator of storm intensity and lightning probability? *Monthly Weather Review*, *122*(8), 1751–1759. https://doi.org/10.1175/1520-0493(1994)122<1751:TVPORR>2.0.CO;2